INVESTIGATION OF THE ATMOSPHERIC OZONE FORMATION POTENTIAL OF PROPYLENE GLYCOL

Final Report to
Philip Morris, USA

by
William P. L. Carter, Dongmin Luo, and Irina L. Malkina

May 2, 1997

College of Engineering
Center for Environmental Research and Technology
University of California
Riverside, California 92521

97-AP-RT8C-002-FR

ABSTRACT

A series of environmental chamber experiments and computer model calculations were carried out to assess the atmospheric ozone formation potential of propylene glycol (PG). The experiments consisted of determining the effects of adding PG on NO oxidation, ozone formation and integrated OH radical levels in simulated model photochemical smog systems. Experiments were carried out using two different surrogate mixtures to represent the reactive organic gases (ROGs) present in the atmosphere, and using differing ROG/NO_x ratios. It was found that PG has a positive effect on ozone formation, and that it does not significantly enhance or inhibit OH radical levels. The rates of consumption of PG in the chamber experiments relative to those of m-xylene corresponded to OH radical rate constant of (2.8±0.6) x 10^{-11} cm^3 $molec^{-1}$ s^{-1}, which is almost a factor of three higher than the previously reported value of Wiedelmann and Zetzch (1982), but is within the experimental uncertainty of the value recently obtained by Aschmann and Atkinson (1997). The observed effects of PG on NO oxidation and O_3 formation were inconsistent with the previously determined lower OH + PG rate constant, and were much better predicted by model simulations using the higher rate constants of Aschmann and Atkinson (1997) as determined in this work.

The PG mechanism with the higher OH + PG rate constant was then used to estimate its ozone impacts for a variety of atmospheric conditions. These were compared with ozone impacts calculated for representative VOCs and for the mixture of all emitted VOCs. The results indicated that the ozone impact of PG was comparable to the average for all VOC emissions.

ACKNOWLEDGEMENTS

The authors gratefully acknowledge Dr. Roger Atkinson for carrying out the OH + propylene glycol measurement as part of his EPA-funded project, and providing us with the results prior to publication. We also acknowledge Mr. Dennis Fitz for assistance in administering this program, Mr. Kurt Bumiller and Ms. Kathalena Smihula for assistance in carrying out the experiments, and Dr. Roger Atkinson for helpful discussions. This work was funded by Philip Morris, USA. However, the opinions and conclusions expressed in this report are entirely those of the primary author, Dr. William P. L. Carter. Mention of trade names or commercial products do not constitute endorsement or recommendation for use.

TABLE OF CONTENTS

LIST OF TABLES

LIST OF FIGURES

INTRODUCTION

Ozone in photochemical smog is formed from the gas-phase reactions of volatile organic compounds (VOCs) and oxides of nitrogen (NO_x) in sunlight. Although Los Angeles has the worst ozone problem in the United States, other areas of the country also have episodes where ozone exceeds the federal air quality standard of 0.12 ppm. Ozone control strategies in the past have focused primarily on VOC controls, though the importance of NO_x control has become recognized in recent years. VOC and NO_x controls have differing effects on ozone formation. NO_x is required for ozone formation, and if the levels of NO_x are low compared to the levels of reactive VOCs, then changing VOC emissions will have relatively little effect on ozone. Since NO_x is removed from the atmosphere more rapidly than VOCs, ozone in areas far downwind from the primary sources tend to be more NO_x limited, and thus less responsive to VOC controls. VOC controls tend to reduce the rate that O_3 is formed when NO_x is present, so VOC controls are the most beneficial in reducing O_3 in the urban source areas, where NO_x is relatively plentiful, and where O_3 yields are determined primarily by how rapidly it is being formed. Because of this, any comprehensive ozone control strategy must involve reduction of emissions of both NO_x and VOCs.

Many different types of VOC compounds are emitted into the atmosphere, each reacting at different rates and having different mechanisms for their reactions. Because of this, they can differ significantly in their effects on ozone formation, or their "reactivity". Some compounds, such as CFCs, do not react in the lower atmosphere at all, and thus make no contribution to ground-level ozone formation. Others, such as methane, react and contribute to ozone formation, but react so slowly that their practical effect on ozone formation is negligible. Obviously, it does not make sense to regulate such compounds as ozone precursors. In recognition of this, the EPA has exempted certain compounds from such regulations on the basis of having "negligible" effects on ozone formation. Although the EPA has no formal policy on what constitutes "negligible" reactivity, in practice it has used the ozone formation potential of ethane as the standard in this regard. This is because ethane is the most reactive of the compounds that the EPA has exempted to date. Therefore, the ozone formation potential of a compound relative to ethane is of particular interest when assessing whether it might be a likely candidate for exemption from regulation as an ozone precursor.

Although presently the EPA does not take into account differences in reactivity among non-exempt compounds in its regulatory policies, model calculations have predicted that non-exempt VOCs can differ by up to 20 times in the amount of ozone they form on a per-mass emitted basis (Carter, 1994). Because of this California utilized "Reactivity Adjustment Factors" to take into account differences in ozone impacts in its Clean Fuel-Low Emissions Vehicle regulations (CARB, 1993), and is now considering how to use reactivity adjustments in its consumer products regulations. The EPA is required under the Clean

Air Act to take reactivity into account in developing consumer product regulations, though it has not yet implemented formal policies in this regard. However, an EPA Senior Science Advisor has proposed a system where non-exempt compounds are classified as "reactive" or "highly reactive", where the borderline is roughly that of the average of all emissions (Dimitriades, 1996). Although the regulatory implications of this is at present uncertain, it is reasonable to expect that in the future compounds judged to be "highly reactive" may be subject to stricter emissions controls than those which are not.

Propylene glycol (PG) is a compound which is used in tobacco processing, and such use may result in its being emitted into the atmosphere. Companies such as Philip Morris whose processes emit this compound have an interest in determining how this impacts the environment. To assess this, Philip Morris contracted with the University of California, Riverside, Center for Environmental Research and Technology (CE-CERT) to carry out an experimental and modeling study of the ozone impacts of propylene glycol. The results of this program are documented in this report.

EXPERIMENTAL AND DATA ANALYSIS METHODS

Overall Experimental Approach

The environmental chamber experiments consisted primarily of measurements of "incremental reactivities" of PG under various conditions. These involve two types of irradiations of model photochemical smog mixtures. The first is a "base case" experiment where a mixture of reactive organic gases (ROGs) representing those present in polluted atmospheres (the "ROG surrogate") is irradiated in the presence of oxides of nitrogen (NO_x) in air. The second is the "test" experiment which consists of repeating the base case irradiation except that the VOC whose reactivity is being assessed is added. The differences between the results of these experiments provide a measure of the atmospheric impact of the test compound, and the difference relative to the amount added is a measure of its reactivity.

To provide data concerning the reactivities of the test compound under varying atmospheric conditions, three types of base case experiments were carried out:

1. Mini-Surrogate Experiments. This base case employed a simplified ROG surrogate and relatively low ROG/NO_x ratios. Low ROG/NO_x ratios represent "maximum incremental reactivity" (MIR) conditions, which are most sensitive to VOC effects. This is useful because it provides a sensitive test for the model, and also because it is most important that the model correctly predict a VOC's reactivity under conditions where the atmosphere is most sensitive to the VOCs. The ROG mini-surrogate mixture employed consisted of ethene, n-hexane, and m-xylene. This same surrogate was employed in our previous studies (Carter et al, 1993a,b; 1995a.), and was found to provide a more sensitive test of the mechanism than the more complex surrogates which more closely represent atmospheric conditions (Carter et al, 1995a). This high sensitivity to mechanistic differences makes the mini-surrogate experiments most useful for mechanism evaluation.

2. Full Surrogate Experiments. This base case employed a more complex ROG surrogate under somewhat higher, though still relatively low, ROG/NO_x conditions. While less sensitive to the mechanism employed, experiments with a more representative ROG surrogate are needed to evaluate the mechanism under conditions that more closely resembling the atmosphere. The ROG surrogate employed was the same as the 8-component "lumped molecule" surrogate as employed in our previous study (Carter et al., 1995a), and consists of n-butane, n-octane, ethene, propene, trans-2-butene, toluene, m-xylene, and formaldehyde. Calculations have indicated that use of this 8-component mixture will give essentially the same results in incremental reactivity experiments as actual ambient mixtures (Carter et al., 1995a).

3. Full Surrogate, low NO_x Experiments. This base case employing the same 8-component lumped molecule surrogate as the full surrogate experiments described above, except that lower NO_x levels (higher

ROG/NO_x ratios) were employed to represent NO_x-limited conditions. Such experiments are necessary to assess the ability of the model to properly simulate reactivities under conditions where NO_x is low. The initial ROG and NO_x reactant concentrations were comparable to those employed in our previous studies (Carter et al. 1995a).

An appropriate set of control and characterization experiments necessary for assuring data quality and characterizing the conditions of the runs for mechanism evaluation were also carried out. These are discussed where relevant in the results or modeling methods sections.

Environmental Chamber

The environmental chamber system employed in this study was the CE-CERT "Dividable Teflon Chamber" (DTC) with a blacklight light source. This consists of two ~5000-liter 2-mil heat-sealed FEP Teflon reaction bags located adjacent to each other and fitted inside an 8'x8'x8' framework, and which uses two diametrically opposed banks of 32 Sylvania 40-W BL black lights as the light source. The lighting system in the DTC was found to provide so much intensity that only half the lights were used for irradiation. The unused black lights were covered with aluminum sheet, and were used to bring the chamber up to the temperature it will encounter during the irradiation before the uncovered lights are turned on. The air conditioner for the chamber room was turned on before and during the experiments. Four air blowers which are located in the bottom of the chamber were used to help cool the chamber as well as mix the contents of the chamber. The CE-CERT DTC is very similar to the Statewide Air Pollution Research Center (SAPRC) DTC which is described in detail elsewhere (Carter et al, 1995a,b).

The DTC is designed to allow simultaneous irradiations of the base case and the test experiments under the same reaction conditions. As indicated above, the chamber is actually two adjacent FEP Teflon reaction bags which can be simultaneously irradiated using the same light source and with the same temperature control system. These are referred to as the two "sides" of the chamber (Side A and Side B) in the subsequent discussion. The sides are interconnected with two ports, each with a box fan, which rapidly exchange their contents to assure that base case reactants have equal concentrations in both sides. In addition, a fan is located in each of the reaction bags to rapidly mix the reactants within each chamber. The ports connecting the two reactors can then be closed to allow separate injections on each side, and separate monitoring of each side. This design is optimized for carrying out incremental reactivity experiments such as those for this program.

Experimental Procedures

The reaction bags were flushed with dry air produced by an AADCO air purification system for 14 hours (6pm-8am) on the nights before experiments. The continuous monitors were connected prior to reactant injection and the data system began logging data from the continuous monitoring systems. The reactants were injected as described below (see also Carter et al, 1993a,, 1995b). The common reactants were injected in both sides simultaneously using a three-way (one inlet and two outlets connected to side

A and B respectively) bulb of 2 liters in the injection line and were well mixed before the chamber was divided. The contents of each side were blown into the other using two box fans located between them. Mixing fans were used to mix the reactants in the chamber during the injection period, but these were turned off prior to the irradiation. The sides were then separated by closing the ports which connected them, after turning all the fans off to allow their pressures to equalize. After that, reactants for specific sides (the test compound in the case of reactivity experiments) were injected and mixed. The irradiation began by turning on the lights and proceeded for 6 hours. After the run, the contents of the chamber were emptied by allowing the bag to collapse, and then was flushed with purified air. The contents of the reactors were vented into a fume hood.

The procedures for injecting the various types of reactants were as follows. The NO and NO_2 were prepared for injection using a high vacuum rack. Known pressures of NO, measured with MKS Baratron capacitance manometers, were expanded into Pyrex bulbs with known volumes, which were then filled with nitrogen (for NO) or oxygen (for NO2). The contents of the bulbs were then flushed into the chamber with AADCO air. The other gas reactants were prepared for injection either using a high vacuum rack or gas-tight syringes, using calculated pressures or volumes to yield the desired concentration in the chamber. The gas reactants in a gas-tight syringe was usually diluted to 100-ml with nitrogen in a syringe. The volatile liquid reactants were injected, using a micro syringe, into a 1-liter Pyrex bulb equipped with stopcocks on each end and a port for the injection of the liquid. The port was then closed and one end of the bulb was attached to the injection port of the chamber and the other to a dry air source. The stopcocks were then opened, and the contents of the bulb were flushed into the chamber with a combination of dry air and heat gun for approximately 5 minutes. Formaldehyde was prepared in a vacuum rack system by heating paraformaldehyde in an evacuated bulb until the pressure corresponded to the desired amount of formaldehyde. The bulb was then closed and detached from the vacuum system and its contents were flushed into the chamber with dry air through the injection port.

Because PG has a high boiling point (184 C) and it may condense in cold spots using usual liquid injection, a heated injection system was used. This was done by placing the desired quantity of PG (typically 10 µl) a three-way (one port for the liquid injection) glass tube which was surrounded with heat tape. The tube was then heated to around 200 C and flushed with purified air at 2 liters/minute for around 15 minutes.

Several preliminary experiments were carried out to determine whether wall absorption of PG may be a problem. The dark decay of PG in the chamber was determined by monitoring it as a function of time for six hours. In a separate experiment, PG, toluene and n-octane were injected into a separate FEP Teflon chamber of approximately the same volume, but which equipped with blacklights. The three compounds were monitored as a function of time in the dark for approximately 100 minutes and then the lights were turned on and they were monitored for an additional two hours.

Analytical Methods

Ozone and nitrogen oxides (NO_x) were continuously monitored using commercially available continuous analyzers with Teflon sample lines inserted directly into the chambers. The sampling lines from each side of the chamber were connected to solenoids which switched from side to side every 10 minutes, so the instruments alternately collected data from each side. Ozone was monitored using a Dasibi 1003AH UV photometric ozone analyzer and NO and total oxides of nitrogen (including HNO_3 and organic nitrates) were monitored using a Teco Model 14B chemiluminescent NO/NO_x monitor. The output of these instruments, along with those from the temperature sensors and the formaldehyde instrument, were attached to a computer data acquisition system, which recorded the data at 10 minutes intervals for ozone, NO and temperature, and at 15 minutes for formaldehyde, using 30 second averaging times. This yielded a sampling interval of 20 minutes for taking data from each side.

The Teco NO/NO_x instrument and the Dasibi CO analyzers were calibrated with certified NO and CO sources using a CSI gas-phase dilution system. It was done prior to each experiment. NO_2 converter efficiency checks were carried out in regular intervals. The ozone analyzer was calibrated against a transfer standard ozone analyzer approximately every three months, and was checked with CSI ozone generator (set to 400 ppb) prior to each experiment. The details of these procedures are discussed elsewhere (Carter et al, 1995b).

Organic reactants other than formaldehyde were measured by gas chromatography with FID and ECD detectors as described elsewhere (Carter et al., 1993a; 1995b). GC samples were taken for analysis after the reactant injection and prior to irradiation, and at intervals from 20 minutes to 30 minutes after the irradiation began. For the analysis of the more volatile compounds, including all of the compounds employed in these experiments except for PG, 100 ml of air from the chamber was withdrawn using a 100 ml gas-tight glass syringe, whose contents were then flushed through 2-3 mil stainless steel or Teflon tube loops attached to the GC with a gas sample valve. For the analysis of PG and also m-xylene, 100 ml of air from the chamber was passed through a glass cartridge filled with Tenax-GC solid absorbent. This tube was then placed in the injector of the GC column, and at 300C to desorb the sample for analysis. These are referred to as the "loop" analysis and "tenax" analysis methods, respectively. M-xylene was monitored using both methods, the m-xylene data from the tenax method was used for most of the data analysis discussed in this report.

Characterization Methods

Three temperature thermocouples for each chamber were used to monitor the chamber temperature. Two were located in the sampling line of continuous analyzers to monitor the temperature in each side, and a third was located in the chamber to monitor chamber temperature. The temperature in these experiment were typically 21-25 C.

The light intensity in the chamber was monitored by periodic NO_2 actinometry experiments utilizing the quartz tube method of Zafonte et al (1977), with the data analysis method modified as discussed by Carter et al. (1995b). The results of these experiments were tracked over time in this chamber since it was first constructed in early 1994, and were fit by a curve where the NO_2 photolysis rate decayed relatively rapidly from its initial values of ~0.31 min^{-1} when the chamber and lights were new, then declining only slowly during the time of these experiments. A curve through the full set of actinometry results predicted NO_2 photolysis rates in the range of 0.193 - 0.195 min^{-1} during the time of these experiments, and the result of the actinometry experiment associated with the runs in this study is consistent with this range. The spectrum of the blacklight light source was measured using a LiCor LI-1200 spectra radiometer, and found to be essentially the same as the general blacklight spectrum recommended by Carter et al (1995b) for use in modeling blacklight chamber experiments.

The dilution in the chamber due to sampling is expected to be small because the flexible reaction bags can collapse as samples are withdrawn for analysis. However, because of small leaks, some dilution occurs with the aging of reaction bags. Information concerning dilution in an experiment can be obtained from relative rates of decay of added VOCs which react with OH radicals with differing rate constants (Carter et al., 1993a; 1995b), or from monitoring CO in CO - NO_x irradiations. The result of the CO - NO_x run carried out during this program indicated negligible dilution, and relative VOC decay data indicated dilution in the range of 0-1% per hour.

Reactivity Data Analysis Methods

As indicated above, most of the experiments for this program consisted of simultaneous irradiation of a "base case" reactive organic gas (ROG) surrogate - NO_x mixture in one of the dual reaction chambers, together with an irradiation, in the other reactor, of the same mixture with PG added. The results are analyzed to yield two measures of VOC reactivity: the effect of the added VOC on the amount of NO reacted plus the amount of ozone formed, and integrated OH radical levels. These are discussed in more detail below.

The first measure of reactivity is the effect of the VOC on the change in the quantity $[O_3]$-[NO], or $([O_3]_t$-$[NO]_t)$-$([O_3]_0$-$[NO]_0)$, which is abbreviated as $d(O_3$-NO) in the subsequent discussion. As discussed elsewhere (e.g., Johnson, 1983; Carter and Atkinson, 1987; Carter and Lurmann, 1990, 1991, Carter et al, 1993a, 1995b,c), this gives a direct measure of the amount of conversion of NO to NO_2 by peroxy radicals formed in the photooxidation reactions, which is the process that is directly responsible for ozone formation in the atmosphere. (Johnson calls it "smog produced" or "SP".) The incremental reactivity of the VOC relative to this quantity, which is calculated for each hour of the experiment, is given by

$$IR[d(O_3\text{-NO})]_t^{VOC} = \frac{d(O_3\text{-NO})_t^{test} - d(O_3\text{-NO})_t^{base}}{[VOC]_0} \qquad (I)$$

where $d(O_3\text{-}NO)_t^{test}$ is the $d(O_3\text{-}NO)$ measured at time t from the experiment where the test VOC was added, $d(O_3\text{-}NO)_t^{base}$ is the corresponding value from the corresponding base case run, and $[VOC]_0$ is the amount of test VOC added. An estimated uncertainty for $IR[d(O_3\text{-}NO)]$ is derived based on assuming an ~3% uncertainty or imprecision in the measured $d(O_3\text{-}NO)$ values. This is consistent with the results of the side equivalency test, where equivalent base case mixtures are irradiated on each side of the chamber.

Note that reactivity relative to $d(O_3\text{-}NO)$ is essentially the same as reactivity relative to O_3 in experiments where O_3 levels are high, because under such conditions $[NO]_t^{base} \approx [NO]_t^{test} \approx 0$, so a change $d(O_3\text{-}NO)$ caused by the test compound is due to the change in O_3 alone. However, $d(O_3\text{-}NO)$ reactivity has the advantage that it provides a useful measure of the effect of the VOC on processes responsible for O_3 formation even in experiments where O_3 formation is suppressed by relatively high NO levels.

The second measure of reactivity is the effect of the VOC on integrated hydroxyl (OH) radical concentrations in the experiment, which is abbreviated as "IntOH" in the subsequent discussion. This is an important factor affecting reactivity because radical levels affect how rapidly all VOCs present, including the base ROG components, react to form ozone. If a compound is present in the experiment which reacts primarily with OH radicals, then the effect of the VOC on OH radicals can be determined by its effect on the rate of decay of that compound. M-xylene is used for this purpose in our experiments, because it is present in all our reactivity experiments as a component of base case surrogate, is consumed only by reaction with OH radicals, and reacts relatively rapidly.

CHEMICAL MECHANISMS AND MODELING METHODS

General Atmospheric Photooxidation Mechanism

The chemical mechanism used in the environmental chamber and atmospheric model simulations in this study is given in Appendix A to this report. This mechanism is based on that documented by Carter (1990), with a number of updates as discussed below. It can explicitly represent a large number of different types of organic compounds, but it lumps together species reacting with similar rate constants and mechanisms in simulations of atmospheric mixtures, and it uses a condensed representation for many of the reactive organic products. The reactions of inorganics, CO, formaldehyde, acetaldehyde, peroxyacetyl nitrate, propionaldehyde, peroxypropionyl nitrate, glyoxal and its PAN analog, methylglyoxal and several other product compounds are represented explicitly. In addition, the reactions of unknown photoreactive products formed in the reactions of aromatic hydrocarbons are represented by model species whose yields and photolysis parameters are adjusted based on fits of model simulations to environmental chamber experiments. A chemical operator approach is used to represent peroxy radical reactions, as discussed in detail by Carter (1990). Generalized reactions with variable rate constants and product yields are used to represent the primary emitted alkane, alkene, aromatic and other VOCs, with rate constants and product yields appropriate for the individual compounds being represented in each simulation). The tables in the Appendix list only those VOCs (or groups of VOCs) used in the simulations in this work. Most of the higher molecular weight oxygenated product species are represented using the "surrogate species" approach, where simpler molecules such as propionaldehyde or 2-butanone are used to represent the reactions of higher molecular weight analogues that are assumed to react similarly.

Several aspects of the Carter (1990) mechanism were updated prior to this work to account for new kinetic and mechanistic information for certain classes of compounds as described by Carter et. al. (1993b) and Carter (1995), and further modifications were made to the uncertain portions of the mechanisms for the aromatic hydrocarbons to satisfactorily simulate results of experiments carried out using differing light sources (Carter et al. 1997). The latest version of the general mechanism is discussed by Carter et al. (1997).

Atmospheric Reactions of Propylene Glycol

Propylene glycol is expected to react in the atmosphere mainly with hydroxyl (OH) radicals. Prior to this work the only available measurement for this rate constant was 1.2×10^{-12} cm^3 $molec^{-1}$ s^{-1}. at 295°K, reported by Wiedelmann and Zetzch (1982), as given by Atkinson (1989). This was measured using an absolute method, involving determining OH decay in the presence of the compound in excess, which might tend to give low values if the compound becomes absorbed on the walls. More recently, using a relative rate method and a large volume chamber where wall absorption is less likely to be a problem, Aschmann and Atkinson (1997) obtained an OH + PG rate constant of 2.23×10^{-11} cm^3 $molec^{-1}$

s^{-1} (relative to 2.36 x 10^{-11} cm^3 $molec^{-1}$ s^{-1} for OH + m-xylene), which is almost a factor of two higher. Although the data of Aschmann and Atkinson (1997) are less likely to be influenced by surface absorption problems, the lower rate constant of Wiedelmann and Zetzch (1982) is in somewhat better agreement with predictions of structure-reactivity estimation methods (Atkinson, 1987). For that reason, both rate constants will be employed in the evaluations of the model predictions against the chamber data.

If the structure-reactivity estimation methods (Atkinson, 1987) are assumed to be reliable for estimating branching rations, then ~70% of the reaction is expected to involve OH attack at the 2-position, resulting in the ultimate formation of hydroxyacetone and the conversion of a single molecule of NO to NO_2, and a regeneration of the OH radical.

$$OH + CH_3CH(OH)CH_2OH \rightarrow H_2O + CH_3C(\cdot)(OH)CH_2OH$$
$$CH_3C(\cdot)(OH)CH_2OH + O_2 \rightarrow HO_2 + CH_3COCH_2OH$$
$$HO_2 + NO \rightarrow NO_2 + OH$$

Most of the remainder of the reaction is expected to involved abstraction from the 1-position, ultimately giving rise to hydroxypropionaldehyde [$CH_3CH(OH)CHO$] through an analogous set of reactions. Reaction at the other positions would occur to only a minor extent, with abstraction from the O-H bonds giving rise to the same products as the two major pathways, though through a somewhat different route. Note that there are no product data to confirm these estimates of relative reaction routes, and the actual branching ratios for these competing processes are somewhat uncertain. However, we would expect hydroxyacetone and hydroxypropionaldehyde formation to be the major processes, with the former being formed in a higher yield than the latter. Test calculations showed that the results of the model simulations of the chamber experiments are not highly sensitive to the relative yields assumed for these two pathways.

The mechanisms used for PG in the model simulations in this work, based on the above considerations, are given in Appendix A. As indicated above, because of the inconsistency between the OH + PG rate constant measurements, calculations were carried out with the OH + PG rate constant varied. Hydroxyacetone and hydroxypropionaldehyde are not represented explicitly in the standard mechanism, and so they are represented in our model simulations by MEK (methyl ethyl ketone) and RCHO (propionaldehyde), respectively. This is consistent with the approach used for the oxygenated products for other VOCs in the mechanism, where MEK represents all higher ketones other than acetone and dicarbonyls, and RCHO represents all C_{3+} mono-aldehydes. Some test calculations were conducted where hydroxyacetone was represented explicitly [using the hydroxyacetone reactions incorporated in the detailed isoprene mechanism of Carter and Atkinson (1996)], and essentially equivalent results were obtained.

Environmental Chamber Simulations

The ability of the chemical mechanisms to appropriately simulate the atmospheric impacts of PG was evaluated by conducting model simulations of the environmental chamber experiments from this study. This requires including in the model appropriate representations of chamber-dependent effects such as wall reactions and characteristics of the light source. The methods used are based on those discussed in detail by Carter and Lurmann (1990, 1991), updated as discussed by Carter et al (1995b,d). The photolysis rates were derived from results of NO_2 actinometry experiments and direct measurements of the spectra of the light source. In the case of the blacklights used in the DTC, the spectrum was assumed to be constant and the blacklight spectrum given by Carter et al (1995b,d) was employed. The thermal rate constants were calculated using the temperatures measured during the experiments, with the small variations in temperature with time during the experiment being taken into account. The computer programs and modeling methods employed are discussed in more detail elsewhere (Carter et al, 1995b). The specific values of the chamber-dependent parameters used in the model simulations of the experiments for this study are given in Appendix A.

Atmospheric Reactivity Simulations

To estimate its effects on ozone formation under conditions more representative of polluted urban atmospheres, incremental reactivities, defined as the change in O_3 caused by adding small amounts of a compound to the emissions, were calculated for ethane, propylene glycol, and several other representative compounds for various simulated atmospheric pollution scenarios. Carter (1994a) used a series of single-day EKMA box model scenarios (EPA, 1984) derived by the EPA to represent 39 different urban ozone exceedence areas around the United States (Baugues, 1990), to develop various reactivity scales to quantify impacts of VOCs on ozone formation in various environments. It was found that NO_x levels are the most important factor affecting differences in relative ozone impacts among VOCs, and that the ranges of relative reactivities in the various scales can be reasonably well represented by ranges in relative reactivities in three "averaged conditions" scenarios representing three different NO_x conditions. These scenarios were derived by averaging the inputs to the 39 EPA scenarios, except for the NO_x emissions. In the "maximum reactivity" scenario, the NO_x inputs were adjusted such that the final O_3 level is most sensitive to changes in VOC emissions; in the "maximum ozone" scenario the NO_x inputs were adjusted to yield the highest maximum O_3 concentration; and in the "equal benefit" scenario the NO_x inputs were adjusted such that relative changes in VOC and NO_x emissions had equal effect on ozone formation. As discussed by Carter (1994a), there represent respectively the high, medium and low ranges of NO_x conditions which are of relevance when assessing VOC control strategies for reducing ozone.

The chemical mechanisms used for these atmospheric simulations were the same as used to simulate the chamber experiments, except that the reactions representing chamber effects were removed, and the reactions for the full variety of VOCs emitted into the scenarios (Carter, 1994a) were represented (see Appendix A). Most of the emitted VOCs (other than the test compound whose reactivity is being calculated) are not represented in the model explicitly, but are represented using lumped model species

whose rate constants and product yield parameters are derived based on the mixture of compounds they represent. The rate constants and mechanistic parameters for the emitted species in the scenarios were the same as those used previously (Carter, 1994a; Carter et al, 1993b), except for the updates to the general mechanism as discussed above (see also Carter et al. 1997). The listings on Appendix A give the lumped model species used to represent the emissions into the scenarios, indicate the types of species each is used to represent, and give their rate constants and product yield parameters.

RESULTS AND DISCUSSION

Results of Preliminary Tests

To provide useful environmental chamber data for evaluating mechanisms for the gas-phase reactions of a compound, it is necessary to be able to reproducibly inject and quantitatively monitor the compound in the gas phase, and it should not be so prone to surface absorption that surface absorption processes significantly affect the results. Prior to carrying out this study, there was some concern about the possibility that propylene glycol may have problems in this regard. Therefore, several preliminary experiments were carried out to assess this.

The analysis of PG and other VOCs by our GC instruments are calibrated by injecting measured amounts of the compounds into a 3200-liter Teflon reaction bag similar to the DTC, measuring the volume of the calibration bag by injecting known amounts of CO and monitoring it with an independently calibrated instrument, and then carrying out repetitive GC analysis for the VOC in the calibration bag. The reproducibility of these calibrations, and the FID response compared to other VOCs, thus provides an indication of our ability to reproducibly inject and monitor the compound in the gas phase.

The results of calibrations of propylene glycol from three separate chamber injections carried out prior to the main series of chamber experiments were as follows:

Date	GC Area response/ppmC	%SD
5/29/96	2.60×10^5	4%
6/3/96	2.59×10^5	5%
6/6/96	2.58×10^5	2%

It can be seen that good reproducibility and precision in the three separate injections were obtained. However, the FID area response on a per carbon basis of 2.6×10^5 is somewhat lower than observed for other compounds; for example, for t-butanol the GC area response per ppmC is 5.0×10^5, and for most hydrocarbons it is around 7×10^5. While this could indicate the possibility of incomplete injection, it is more likely that the FID response is less because the PG is more oxidized than hydrocarbons or t-butanol. For example, the area response per ppmC for acetaldehyde is even lower at 1.4×10^5.

To determine whether surface absorption was occurring at a measurable rate once the PG was injected into the gas phase, its dark decay was determined by monitoring it as a function of time for six hours after injection into 3200-liter calibration bag. No observable decay was observed over a 6-hour period.

Figure 1. Concentration - time plots of propylene glycol and tracer compounds in the propylene glycol dark and light decay test experiment.

In a separate experiment, the PG, along with toluene and n-octane, were injected into a different FTP Teflon chamber of approximately the same volume but equipped with blacklights. The three compounds were monitored as a function of time in the dark for approximately 100 minutes and then the lights were turned on and they were monitored for an additional two hours. The resulting concentration-time data obtained for PG and the tracer compounds in this experiment are shown on Figure 1. It can be seen that over a ~100 minute period there was only a gradual decline in concentration of all three compounds in the dark, which can be attributed to dilution at a rate of 1.3%/hour, due to small leaks in the reactor used. (This reactor is not normally used for calibrations, and holes made in it for another study had to be patched before carrying out this test.) This indicates that this compound, once in the gas phase, is not lost to wall absorption to a measurable extent. The relatively rapid decay of PG after the lights are turned on is attributed to photochemical reaction, though the possibility of light-induced heterogeneous decay cannot be completely eliminated.

Based on the results of these preliminary tests, it was concluded that we should be able to successfully obtain quantitative information concerning the gas-phase reactions of PG in environmental chamber experiments.

Summary of Environmental Chamber Experiments

Table 1 gives a chronological listing of the environmental chamber experiments carried out for this program once the preliminary tests, discussed above, were completed. These consisted primarily of incremental reactivity experiments, whose conditions are summarized on Table 2, and whose results are

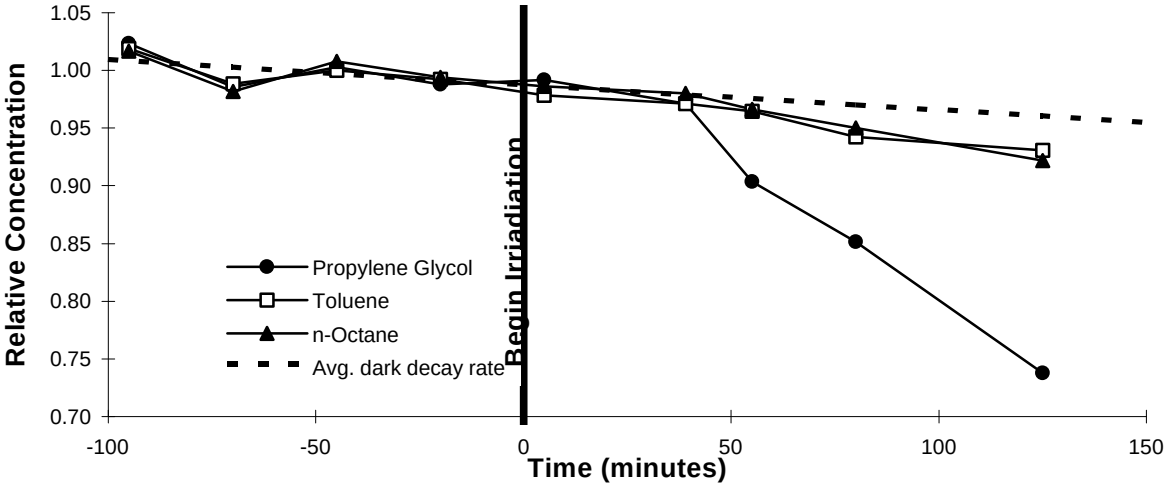

Figure 1. Concentration - time plots of propylene glycol and tracer compounds in the propylene glycol dark and light decay test experiment.

Table 1. Chronological listing of the environmental chamber experiments carried out to assess the reactivity of propylene glycol.

Run	Date	Run Title	Description	Comments
DTC383	7/16/96	CO + NOx	Control run to measure chamber radical source and chamber dilution.	NO oxidation rate somewhat faster than predicted by standard chamber model, but results within normal variability.
DTC384	7/19/96	n-Butane + NOx	Control run to measure chamber radical source and for comparison with other n-butane runs.	No n-butane data available, so initial n-butane had to be estimated. Results consistent with predictions of standard chamber model.
DTC385	7/23/96	Mini-Surrogate + Propylene Glycol (A)	See Table 2.	See Table 2 and Figure 2.
DTC386	7/24/96	Full Surrogate + Propylene Glycol (B)	See Table 2.	See Table 2 and Figure 3.
DTC388	7/30/96	Low NOx Full Surrogate + Propylene Glycol (A)	See Table 2.	See Table 2 and Figure 4..
DTC389	7/31/96	Mini-Surrogate + Propylene Glycol (B)	See Table 2.	See Table 2 and Figure 2.
DTC390	8/1/96	Full Surrogate + Propylene Glycol (A)	See Table 2.	See Table 2 and Figure 3.
DTC391	8/2/96	Low NOx Full Surrogate + Propylene Glycol (B)	See Table 2.	See Table 2 and Figure 4..
DTC392	8/5/96	NO_2 Actinometry	Measurement of NO_2 photolysis rate by quartz tube method.	Measured NO_2 photolysis rate was 0.191 min^{-1}, in good agreement with trend from other actinometry results.
DTC393	8/6/96	Propene - NOx	Standard propene run to verify reproducibility of conditions in the chamber.	Results were in good agreement with model predictions. Good side equivalency observed.

Table 2. Summary of conditions and results of the incremental reactivity experiments.

shown on Figures 2-4. The results of these experiments will be discussed in the following two sections. In addition, several characterization runs were carried out to determine the chamber-dependent inputs needed for the model simulations of the experiments, and control experiments were conducted to assure consistency with previous results.

Table 1 summarizes relevant results from these characterization and control runs. Their results were as expected based on our previous experience with these and similar chambers in our laboratories (Carter et al., 1995b and references therein). Good side equivalency was observed when equivalent surrogate - NO_x (not shown), propene - NO_x, CO - NO_x, or n-butane - NO_x mixtures were simultaneously irradiated in the dual reactors. The results of the CO - NO_x and n-butane - NO_x experiments, which are highly sensitive to the magnitude of the chamber radical source assumed in the model (see Table A-4 in Appendix A), were sufficiently well simulated by the model to indicate that the model was appropriately representing this effect for these runs. The actinometry results agreed with the extrapolated values based on results of previous determinations (see Table A-4).

Some problems encountered in the GC analysis method normally used for n-octane, toluene, and m-xylene which affected these data for most of the reactivity experiments for this program. A change was made to the instrument which introduced a problem causing a deterioration in the quality of the data from that instrument until the problem was corrected, and some of the data for these compounds had to

Table 2. Summary of conditions and results of the incremental reactivity experiments.

Run	Avg. T	Initial Reactants (ppm)			t=6 d(O_3-NO) (ppm)			kOH^{PG} / $kOH^{m\text{-}Xyl}$
	(deg K)	NOx	Surg [a]	Pr.Glycl	Base	Test	IR [b]	
Mini-Surrogate								
DTC-385 (A)	298	0.38	4.64	2.58	0.50	0.94	0.17	0.93 ± 0.04
DTC-389 (B)	299	0.37	5.88	0.99	0.56	0.78	0.22	1.10 ± 0.03
Full Surrogate - High NOx								
DTC-386 (B)	298	0.28	3.74	1.01	0.52	0.76	0.24	1.26 ± 0.08
DTC-390 (A)	297	0.27	3.76	0.74	0.52	0.75	0.31	1.46 ± 0.08
Full Surrogate - Low NOx								
DTC-388 (A)	298	0.11	3.74	1.07	0.34	0.43	0.09	1.28 ± 0.13
DTC-391 (B)	297	0.12	3.64	0.53	0.35	0.41	0.11	0.90 ± 0.14

Notes

[a] Total base ROG surrogate in ppmC.

[b] Incremental reactivity

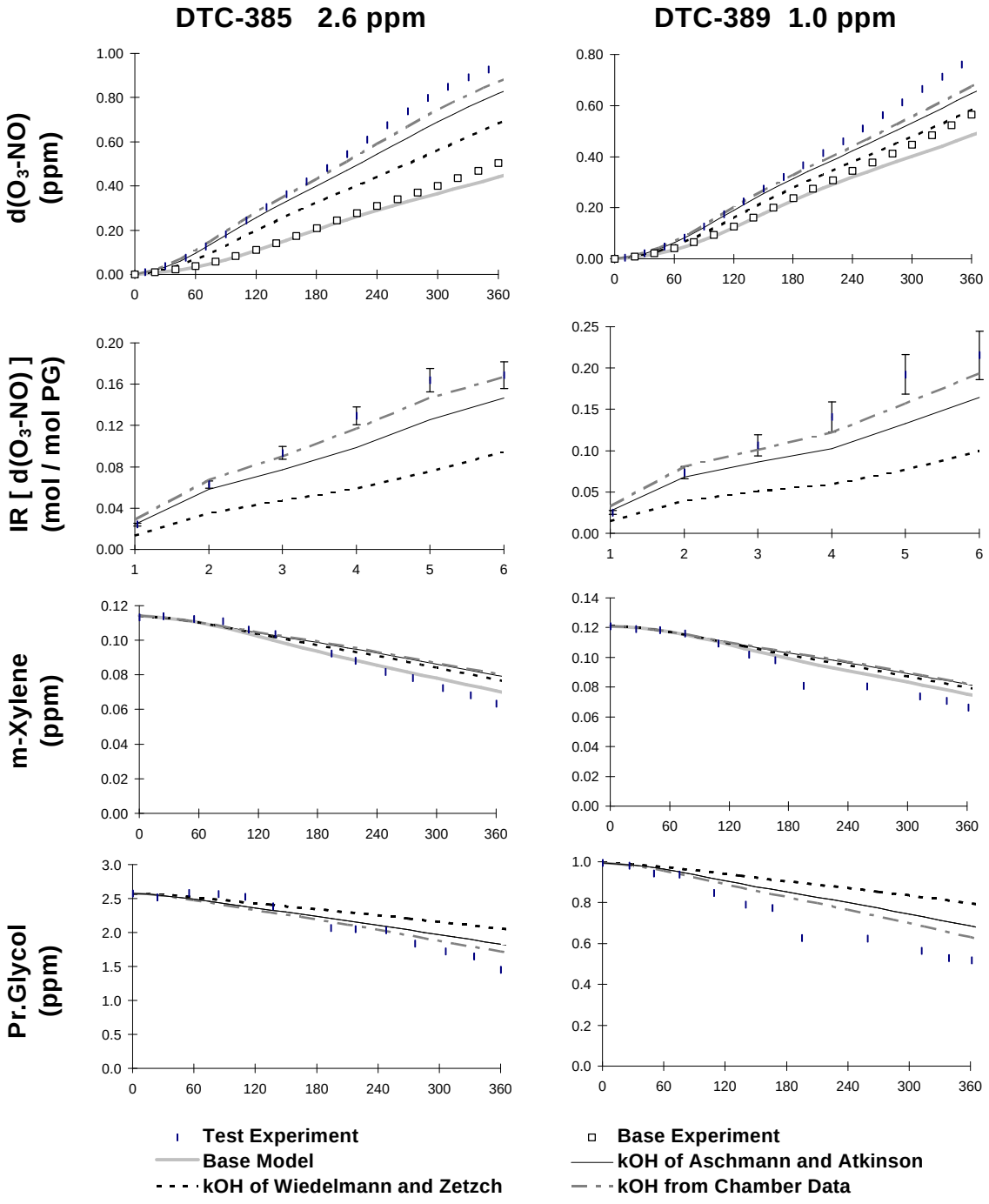

Figure 2. Time series plots of experimental and calculated results of thereactivity experiments using the mini-surrogate.

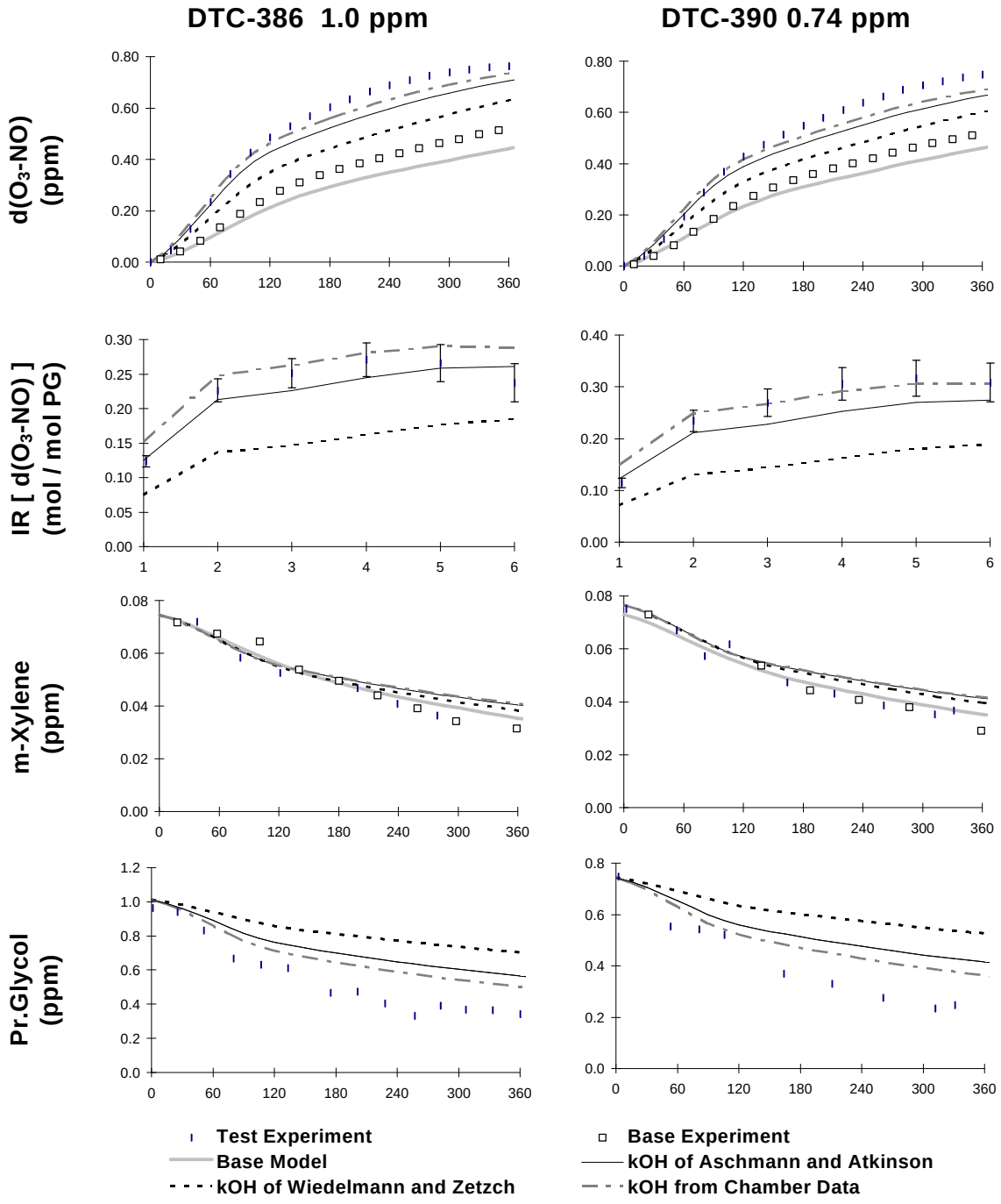

Figure 3. Time series plots of experimental and calculated results of thereactivity experiments using the full surrogate.

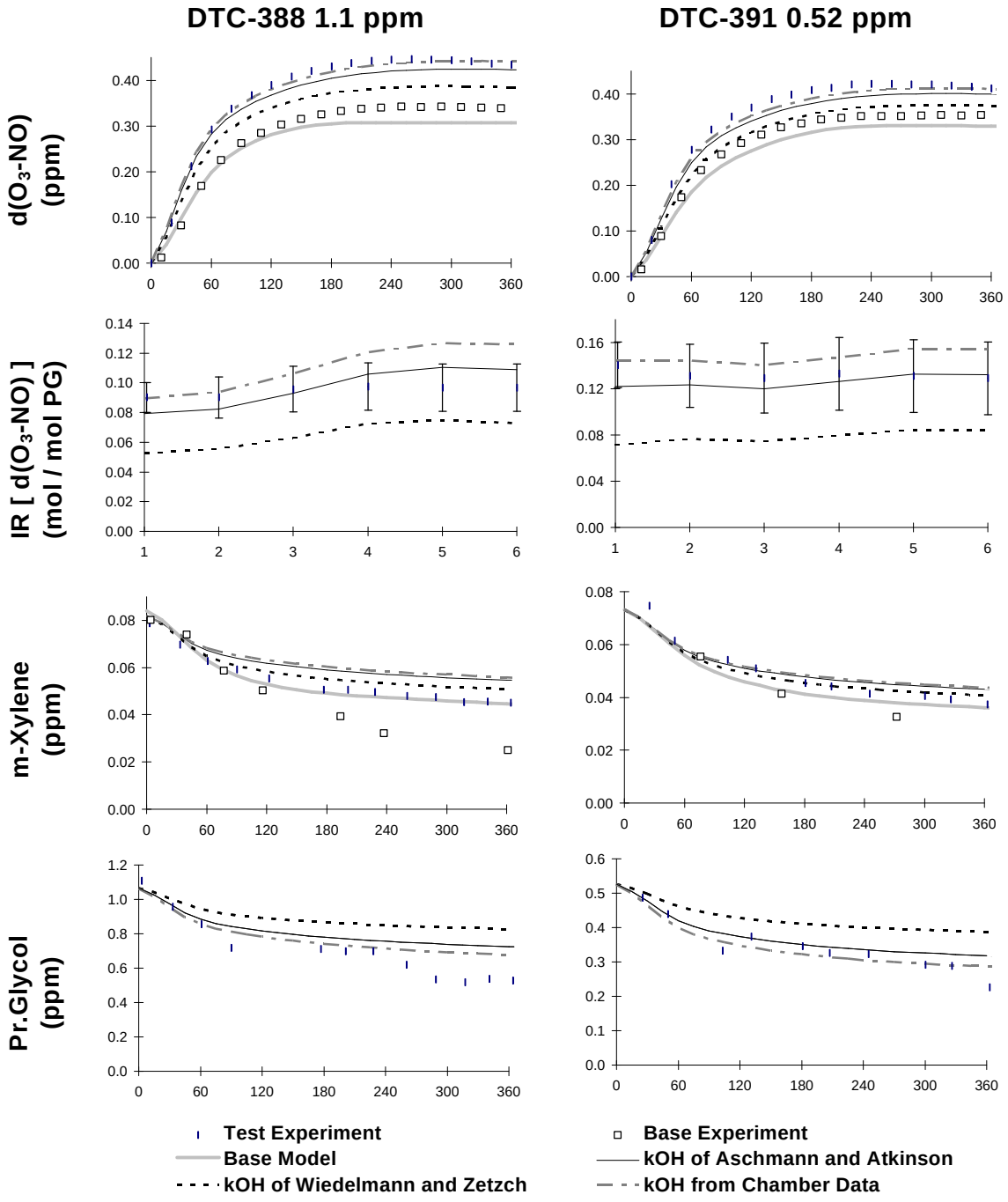

Figure 4. Time series plots of experimental and calculated results of thereactivity experiments using the low$_x$NO full surrogate.

be rejected. Fortunately, experience with many of these type of runs at our laboratories indicated that very reproducible injections of these surrogate components are obtained in these reactivity experiments, so averages of initial concentrations from other runs of the same type could be used for determining initial conditions for modeling purposes without introducing significant uncertainties. In addition, reasonably high quality data for m-xylene was also obtained from the GC instrument used for the Tenax analysis of propylene glycol, so reliable m-xylene data were always available for the added PG experiments. However, because such tenax samples were not taken in the base case runs, in some of the reactivity experiments reliable m-xylene data are only available for the added PG side.

Propylene Glycol Consumption Rates and OH Radical Rate Constant Determination

Figures 2-3 show that the consumption rates of propylene glycol during the reactivity experiments is comparable to those for m-xylene, the base ROG component whose rate of consumption is used to estimate OH radical levels. Since both PG and m-xylene are expected to be consumed in these experiments primarily by reaction with OH radicals, since dilution in these experiments is small compared to the amounts of PG and m-xylene reacted, and since the preliminary experiments indicate that wall losses of PG are insignificant (at least in the dark), then these data can then be used to obtain a measurement of the rate constant ratio for the reaction of OH radicals with PG relative to their reaction with m-xylene. The OH + PG rate constant can then be placed on an absolute basis using the known OH + m-xylene rate constant of 2.36 x 10^{-11} cm^3 $molec^{-1}$ s^{-1} (Atkinson, 1989), and compared with the results of the OH + PG determinations of Wiedelmann and Zetzch (1982) and Aschmann and Atkinson (1997).

If PG and m-Xylene are consumed only by reaction with OH radicals, and possibly also to a small extent by dilution, then their rates of consumption are given by

$$\frac{d\ ln[m\text{-}Xyl]}{dt} = kOH^{m\text{-}Xyl}\ [OH]_t + D$$

$$\frac{d\ ln[PG]}{dt} = kOH^{PG}\ [OH]_t + D$$

where [m-Xyl] and [PG] are the concentration of these species at time t, $kOH^{m\text{-}Xyl}$ and kOH^{PG} are their respective OH radical rate constants, $[OH]_t$ is the instantaneous OH radical rate constant concentration, and D is the dilution rate. Integrating these and re-arranging yields,

$$ln(\frac{[PG]_0}{[PG]_t}) = (\frac{kOH^{PG}}{kOH^{m\text{-}Xyl}})\ ln(\frac{[m\text{-}Xyl]_0}{[m\text{-}Xyl]_t}) + Dt\ (1 - \frac{kOH^{PG}}{kOH^{m\text{-}Xyl}})$$

where $[m\text{-}Xyl]_0$, $[PG]_0$, $[m\text{-}Xyl]_t$, and $[PG]_t$ are the initial and time=t m-xylene and PG concentrations, respectively. Since dilution is small compared to the rates of consumption of PG and m-xylene, and since $kOH^{PG}/kOH^{n\text{-}Xyl} \approx 1$, then the latter term can be neglected, and

$$\ln\left(\frac{[PG]_0}{[PG]_t}\right) \approx \left(\frac{kOH^{PG}}{kOH^{m\text{-}Xyl}}\right) \ln\left(\frac{[m\text{-}Xyl]_0}{[m\text{-}Xyl]_t}\right) \qquad (II)$$

Thus plots of $\ln([PG]_t/[PG]_0)$ vs $\ln([m\text{-}Xyl]_t/[m\text{-}Xyl]_0)$ should yield straight lines with near-zero intercepts and a slope equal to the OH radical rate constant ratio.

Note that Aschmann and Atkinson (1997) used essentially the same method to determine the OH + PG rate constant, and also used m-xylene as the reference compound. The main difference is that in their experiments the photolysis of methyl nitrite was added to provide the OH radical source, rather than the photochemical smog simulation system used in this study. Methyl nitrite photolysis has the advantage of providing much higher OH radical levels than occur in photochemical smog simulation systems, allowing the reaction to proceed much more rapidly, so the irradiations typically take less than 30 minutes rather than the 6 hours for our smog simulations, and generally higher amounts of reaction are obtained. See Atkinson (1989), and references therein, for a more detailed discussion of the methyl nitrite photolysis method for determining relative OH radical rate constants.

Table 2 shows the $kOH^{PG}/kOH^{n\text{-}Xyl}$ ratios obtained from the slopes of Equation (II) for our experiments, together with (one σ) standard deviations of the slopes. It can be seen that similar results are obtained from the various experiments, with the weighed average being 1.09±0.15, and the unweighed average being 1.16±0.22. These are in fair agreement with the $kOH^{PG}/kOH^{n\text{-}Xyl}$ ratio of 0.95±0.05 determined by Aschmann and Atkinson (1997), being~15-20% higher, but just within the uncertainty range of our determination. Note the greater precision of the Aschmann and Atkinson (1997) data, due to an inherently greater precision in the GC analysis method they employed, and the larger extent of reaction obtained in the methyl nitrite photolysis system.

Note that in principle plots of equation (II) can be used to combine data from all the experiments, to reduce the effects of imprecision of the data and provide a more precise measurement of the rate constant ratio. However, strictly speaking, plots of Equation (II) may not necessarily have zero intercepts because of imprecision in the measured initial concentrations. This can be taken into account by adding a term

$$Error^0_{run} = \left(\frac{kOH^{PG}}{kOH^{m\text{-}Xyl}}\right) \ln\left(\frac{[m\text{-}Xyl]_0^{true}}{[m\text{-}Xyl]_0^{meas}}\right) - \ln\left(\frac{[PG]_0^{true}}{[PG]_0^{meas}}\right)$$

to yield

$$\ln\left(\frac{[PG]_0}{[PG]_t}\right) + Error^0_{run} \approx \left(\frac{kOH^{PG}}{kOH^{m\text{-}Xyl}}\right) \ln\left(\frac{[m\text{-}Xyl]_0}{[m\text{-}Xyl]_t}\right) \qquad (III)$$

where $Error^0_{run}$ is an unknown quantity which is different for each run, but which can be determined by least squares analysis methods. Thus, plots of $\ln([PG]_t/[PG]_0)$ - $Error^0_{run}$ vs $\ln([m\text{-}Xyl]_t/[m\text{-}Xyl]_0)$ should yield a straight line with slope of the rate constant ratio and a true zero intercept.

Figure 5 shows plots of Equation (III) for all the reactivity experiments from this study, where the $Error^0_{run}$ values were determined, together with the $kOH^{PG}/kOH^{m\text{-}Xyl}$ ratio, by minimizing the least squares differences between the two sides of Equation III. A line with slope equal to the best fit ratio, or

$$kOH^{PG}/kOH^{m\text{-}Xyl} = 1.18$$

is also shown, along with a line corresponding to the rate constant ratio measured by Aschmann and Atkinson (1997). It can be seen that reasonably good fits to the expected straight line is obtained. Based on the run-to-run variability of the rate constant ratio (shown on Table 2), we estimate the overall uncertainty of this rate constant ratio determination to be ±20%. Using the OH + m-xylene OH rate constant of 2.36×10^{-11} cm^3 $molec^{-1}$ s^{-1} (Atkinson, 1989) for the reference compound yields an OH + PG rate constant of

$$kOH^{PG} = (2.8 \pm 0.6) \times 10^{-11} \text{ cm}^3 \text{ molec}^{-1} \text{ s}^{-1}$$

at 297-299 K.

This is 26% higher than the kOH^{PG} of $(2.2\pm0.2) \times 10^{-11}$ cm^3 $molec^{-1}$ s^{-1} derived from the data of Aschmann and Atkinson (1997), using the same rate constant for the reference reaction, but can be considered to be within the uncertainty of our determination. Note that because of the longer reaction times in our chamber experiments compared to the methyl nitrite photolysis system of Aschmann and Atkinson (1997), there is a greater chance for a non-negligible contribution due to wall absorption in our system. Although the preliminary experiments indicate that removal of PG from the gas phase due to absorption is not a major factor, it may be enough to account for the ~25% higher apparent PG consumption rate in our experiments. In addition, the possibility of some type of enhanced light-induced decay has not been ruled out.

However, the discrepancy between our data and that of Aschmann and Atkinson (1997) is minor compared to the factor of two difference between these relative rate measurements and the 295°K value of 1.2×10^{-12} cm^3 $molec^{-1}$ s^{-1} determined by Wiedelmann and Zetzch (1982) using an absolute method. We have no obvious explanation for the large magnitude of the discrepancies between this and the relative data, though the directional differences are consistent with the possible biases inherent in each method when applied to potentially "sticky" compounds such as PG. If PG had a tendency to undergo heterogeneous absorption on the walls of our chamber during the 6-hour experiments, it would result in our obtaining OH rate constants which are too high, as indicated above. The slightly higher rate constant obtained in our experiments (with the longer reaction times) compared to methyl nitrite photolysis system

Figure 5. Plots of Equation (III) for all the propylene glycol reactivity chamber experiments.

of Aschmann and Atkinson (1997) suggest that this may be a factor, though not to a major extent. The absolute methods of Wiedelmann and Zetzch (1982) involve monitoring OH decay in the presence of excess PG in a flow system, and if surface absorption results in steady state gas-phase concentrations of PG being lower than expected, then low rate constants would be obtained. However, the Zetzch group generally obtains reliable data for most other compounds they study (e.g., Atkinson, 1989; Atkinson, private communication, 1996), so a factor of >2 error in one of their determinations is unexpected.

To determine which of these rate constants is more consistent with our ozone reactivity data, or whether the data are better fit with an intermediate value, the model simulations of the PG reactivity experiments were carried out using the rate constants of Wiedelmann and Zetzch (1982), Atkinson and Aschmann (1997) and that determined from the PG decay observed in our chamber experiments.

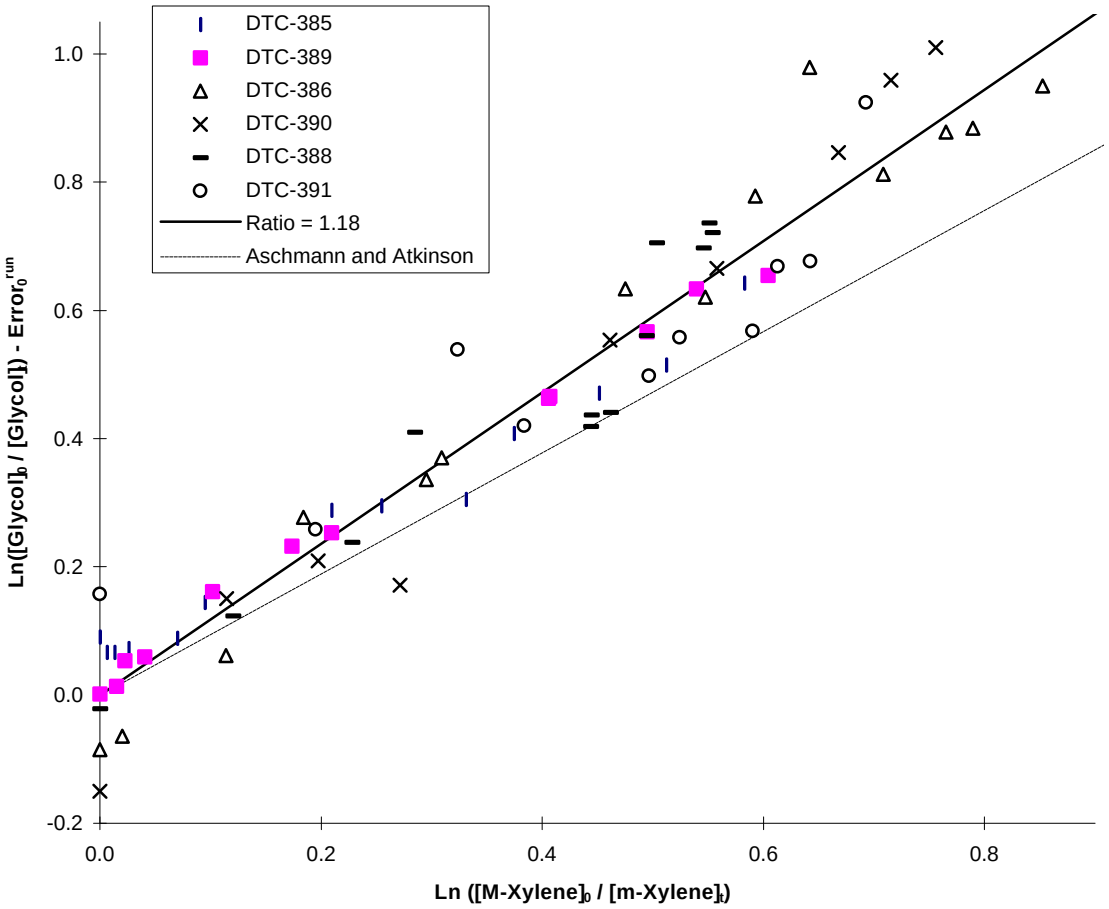

Figure 5. Plots of Equation (III) for all the propylene glycol reactivity chamber experiments.

Results of The Reactivity Experiments and Mechanism Evaluations

Summaries of the conditions for the incremental reactivity experiments are given on Table 2, above, and Figures 2, 3 and 4 give time series plots for relevant measurements used for mechanism evaluation for the mini-surrogate, full surrogate and low-NO_x full surrogate experiments, respectively. These include concentrations of d(O_3-NO) and m-xylene in the base case and test experiments, concentrations of PG in the test experiment, and the d(O_3-NO) incremental reactivities derived from the differences between the two sides. Results of model calculations, with varying OH + PG rate constants, are also shown in these figures.

Table 2 and Figures 2-5 show that PG has a positive effect on NO oxidation and ozone formation in all experiments and at all times in the experiments. PG was not found to have a measurable effect on OH radicals in the moderate NO_x full surrogate experiments, and the m-xylene decay rates observed in the added PG sides of the mini-surrogate reactivity runs are well within the range generally observed for many base case mini-surrogate experiments where reliable m-xylene data were available. This indicates that the reactions of PG involves neither significant radical inhibition or radical initiation processes, in contrast to higher molecular weight alkanes which tend to be radical inhibitors, and compounds like olefins or aromatics which tend to enhance radical levels (Carter et al, 1993a, 1995a). Inhibition of OH radial levels is observed in the latter stages of the low NO_x full surrogate runs, but this radical inhibition under low NO_x conditions is characteristic of all reactive VOCs except for strong radical initiators, and is attributed to the general characteristics of low NO_x conditions (Carter et al, 1995a).

Figures 2-4 also show the results of the model simulations of the reactivity experiments, using the mechanisms with the various OH + PG rate constants. All mechanisms correctly predict that PG has only a small effect on OH radical levels except in the low NO_x experiments, but significantly differ in their predictions of the effects of PG on ozone formation and NO oxidation. The mechanism using the low OH + PG rate constant Wiedelmann and Zetzch (1982) significantly underpredict the effects of PG on d(O_3-NO) in all experiments, particularly in the lower NO_x runs which are most sensitive to mechanism differences. On the other hand, the mechanism using the OH + PG rate constant derived from the observed PG decay rates not only (as expected) gives much better fits to the PG decay rates, it also gives good predictions of the effects of PG on NO oxidation and ozone formation. The mechanism with the slightly lower rate constant of Aschmann and Atkinson (1997) gives similar results, though it tends to underpredict the effects of PG on d(O_3-NO) in the mini-surrogate runs, but give slightly better fits to the d(O_3-NO) effects in the low NO_x full surrogate experiments. This tends to suggest that the higher OH + PG rate constants derived from the relative rate methods in fact reflect their true gas-phase reaction rates, since the wall absorption processes would not explain the relatively large effects of PG on ozone formation and NO oxidation which was observed in our experiments.

Of course, the possibility that the lower OH + PG rate constant may be correct has not been totally ruled out, since the underprediction of PG's reactivity caused by assuming this rate constant may be due

to other errors in the mechanism. However, it is difficult to see how this could be the case. Formation of radical initiating products cannot explain the discrepancy, since this would cause enhanced effects of PG on OH radical levels which are not observed. Representing hydroxyacetone explicitly [as it is in our detailed isoprene mechanism (Carter and Atkinson 1996)] is not sufficient to account for the discrepancies in the mini-surrogate runs and does not significantly effect O_3 predictions in the full surrogate runs. More NO to NO_2 conversions in PG's initial reactions are unlikely, since most of the reaction is expected to occur at a hydrogen with an α-OH group, and the assumed mechanism in this is consistent with both product (Atkinson, 1990, and references therein) and reactivity (Carter et al, 1993a) data for a number of other alcohols. The effects of PG on d(O_3-NO) could be explained if all the OH reaction occurred at the CH_3 group, since an additional NO to NO_2 conversion would be expected to occur in the subsequent reaction, resulting ultimately in the formation of formaldehyde and glycolaldehyde,

$$OH + CH_3CHOHCH_2OH \rightarrow \cdot CH_2CHOHCH_2OH + H_2O$$
$$\cdot CH_2CHOHCH_2OH + O_2 \rightarrow \cdot OOCH_2CHOHCH_2OH$$
$$\cdot OOCH_2CHOHCH_2OH + NO \rightarrow \cdot OCH_2CHOHCH_2OH$$
$$OCH_2CHOHCH_2OH \rightarrow HCHO + \cdot CHOHCH_2OH$$
$$\cdot CHOHCH_2OH + O_2 \rightarrow HO_2 + HOCH_2CHO$$

However, this mechanism predicts that PG causes large enhancements to the formaldehyde yields which are not observed. In addition, based on structure-reactivity considerations (Kwok and Atkinson, 1995; Atkinson, 1997) it is expected that only a small fraction of the reaction would occur at the methyl group.

Therefore, we conclude that the OH + PG rate constants derived using the relative rate method are more likely to be correct, and the low value reported by Wiedelmann and Zetzch (1982) are almost certainly low. Although the chamber data are slightly more consistent with an OH + PG rate constant which is ~25% higher than that determined by Aschmann and Atkinson (1997), the model using the Aschmann and Atkinson (1997) rate constant is probably not outside the uncertainties involved with modeling incremental reactivity experiments (e.g., see Carter, 1995). Since the conditions of our experiments are not optimized for obtaining kinetic data, and we feel that the Aschmann and Atkinson (1997) are more precise and less likely to have complications due to wall absorption, we believe it is more appropriate to use the Aschmann and Atkinson (1997) rate constant for atmospheric modeling purposes.

ATMOSPHERIC REACTIVITY ESTIMATES

Incremental reactivities of VOCs have been shown to be highly dependent on environmental conditions, so reactivities measured in environmental chamber experiments cannot necessarily be assumed to be exactly the same as those under atmospheric conditions (Carter and Atkinson, 1989a; Carter et al, 1995a). The only method available to obtain quantitative estimates of incremental reactivities of VOCs in ambient air pollution episodes is to conduct airshed model simulations of the episodes. Since these simulations cannot be any more reliable than the chemical mechanisms used, the major objective of this program was to assess the reliability of the propylene glycol mechanism for use in such simulations. This was discussed in the previous sections. In this section, we discuss the results of model simulations of its incremental reactivities in a variety of model scenarios representing ozone exceedence episodes in various areas in the United States (Baugues, 1990), and compare the results to incremental reactivities calculated for ethane, the compound used by the EPA as the criterion for determining "negligible" reactivity, for the mixture representing total ROG emissions from all sources, and for other selected VOCs. Because the data from our experiments are reasonably consistent with the mechanism using the OH + PG rate constant of Aschmann and Atkinson (1997), that was the mechanism used in the atmospheric reactivity calculations for PG. However, the effect of assuming the ~25% higher rate constant derived from the PG decay rates in our experiments was also examined.

Scenarios Used for Reactivity Assessment

The set of airshed scenarios employed to assess the PG reactivity for this study is the same as those used for calculating the MIR and other reactivity scales (Carter, 1994a; Carter et al, 1993b). The objective is to use a set of scenarios which represents, as much as possible, a comprehensive distribution of the environmental conditions where unacceptable levels of ozone are formed. Although a set of scenarios has not been developed for the specific purpose of VOC reactivity assessment, the EPA developed an extensive set of scenarios for conducting analyses of effects of ROG and NO_x controls on ozone formation using the Empirical Kinetic Modeling Approach (EKMA) (Gipson et al., 1981; Gipson and Freas, 1983; EPA, 1984; Gery et al., 1987; Baugues, 1990). The EKMA approach involves the use of single-cell box models to simulate how the ozone formation in one day episodes is affected by changes in ROG and NO_x inputs. Although single-cell models cannot represent realistic pollution episodes in great detail, they can represent dynamic injection of pollutants, time-varying changes of inversion heights, entrainment of pollutants from aloft as the inversion height raises, and time-varying photolysis rates, temperatures, and humidities (Gipson and Freas, 1981; EPA, 1984; Gipson, 1984; Hogo and Gery, 1988). Thus, they can be used to simulate a wide range of the chemical conditions which affect ozone formation from ROG and NO_x, and which affect VOC reactivity. Therefore, at least to the extent they are suitable for their intended purpose, an appropriate set of EKMA scenarios should also be suitable for assessing reactivities over a wide range of conditions.

Base Case Scenarios

The set of EKMA scenarios used in this study were developed by the United States EPA for assessing how various ROG and NO_x control strategies would affect ozone nonattainment in various areas of the country (Baugues, 1990). The characteristics of these scenarios and the methods used to derive their input data are described in more detail elsewhere (Baugues, 1990; Carter, 1993; Carter, 1994b). Briefly, 39 urban areas in the United States were selected based on geographical representativeness of ozone nonattainment areas and data availability, and a representative high ozone episode was selected for each. The initial NMOC and NO_x concentrations, the aloft O_3 concentrations, and the mixing height inputs were based on measurement data for the various areas, the hourly emissions in the scenarios were obtained from the National Acid Precipitation Assessment Program emissions inventory (Baugues, 1990), and biogenic emissions were also included. Table 3 gives a summary of the urban areas represented and other selected characteristics of the scenarios.

Several changes to the scenario inputs were made based on discussions with the California ARB staff and others (Carter, 1993; 1994b). Two percent of the initial NO_x and 0.1% of the emitted NO_x in all the scenarios was assumed to be in the form of HONO. The photolysis rates were calculated using solar light intensities and spectra calculated by Jeffries (1991) for 640 meters, the approximate mid-point of the mixed layer during daylight hours. The composition of the NMOCs entrained from aloft was based on the analysis of Jeffries et al (1989). The composition of the initial and emitted reactive organics was derived as discussed below. Complete listings of the input data for the scenarios are given elsewhere (Carter, 1993, 1994b).

This set of 39 EKMA scenarios are referred to as "base case" to distinguish them from the scenarios derived from them by adjusting NO_x inputs to yield standard conditions of NO_x availability as discussed below. No claim is made as to the accuracy of these scenarios in representing any real episode, but they are a result of an effort to represent, as accurately as possible given the available data and the limitations of the formulation of the EKMA model, the range of conditions occurring in urban areas throughout the United States. When developing general reactivity scales it is more important that the scenarios employed represent a realistic distribution of chemical conditions than accurately representing the details of any one particular episode.

The Base ROG mixture is the mixture of reactive organic gases used to represent the chemical composition of the initial and emitted anthropogenic reactive organic gases from all sources in the scenarios. Consistent with the approach used in the original EPA scenarios, the same mixture was used for all scenarios. The speciation for this mixture was derived by Croes (1991) based on an analysis of the EPA database (Jeffries et al. 1989) for the hydrocarbons and the 1987 Southern California Air Quality Study (SCAQS) database for the oxygenates (Croes et al., 1994; Lurmann et al., 1992). This mixture consists of 52% (by carbon) alkanes, 15% alkenes, 27% aromatics, 1% formaldehyde, 2% higher

Table 3. Summary of conditions of base case scenarios used for atmospheric reactivity assessment.

City, State	Calc. Max O_3 (ppb)	ROG /NO_x	NO_x /NO_x^{MOR}	Final Height (km)	Init.+Emit Base ROG (mmol m^{-2})	Aloft O_3 (ppb)
Atlanta, GA	174	7.3	0.7	2.1	12	63
Austin, TX	171	9.3	0.5	2.1	11	85
Baltimore, MD	304	5.2	1.1	1.2	17	84
Baton Rouge, LA	235	6.8	1.0	1.0	11	62
Birmingham, AL	233	6.9	0.6	1.8	13	81
Boston, MA	191	6.5	0.6	2.6	14	105
Charlotte, NC	142	7.8	0.3	3.0	7	92
Chicago, IL	273	11.6	0.5	1.4	25	40
Cincinnati, OH	192	6.4	0.8	2.8	17	70
Cleveland, OH	239	6.6	1.0	1.7	16	89
Dallas, TX	192	4.7	1.3	2.3	18	75
Denver, CO	195	6.3	1.2	3.4	29	57
Detroit, MI	229	6.8	0.8	1.8	17	68
El Paso, TX	177	6.6	1.1	2.0	12	65
Hartford, CT	166	8.4	0.5	2.3	11	78
Houston, TX	291	6.1	1.0	1.7	25	65
Indianapolis, IN	201	6.6	0.9	1.7	12	52
Jacksonville, FL	152	7.6	0.7	1.5	8	40
Kansas City, MO	151	7.1	0.6	2.2	9	65
Lake Charles, LA	282	7.4	0.7	0.5	7	40
Los Angeles, CA	546	7.6	1.0	0.5	23	100
Louisville, KY	203	5.5	0.9	2.5	14	75
Memphis, TN	218	6.8	0.7	1.8	15	58
Miami, FL	131	9.6	0.4	2.7	9	57
Nashville, TN	163	8.1	0.5	1.6	7	50
New York, NY	350	8.1	0.8	1.5	39	103
Philadelphia, PA	230	6.2	1.0	1.8	19	53
Phoenix, AZ	258	7.6	1.0	3.3	40	60
Portland, OR	161	6.5	0.7	1.6	6	66
Richmond, VA	225	6.2	0.8	1.9	16	64
Sacramento, CA	194	6.6	0.9	1.1	7	60
St Louis, MO	301	6.1	1.1	1.6	26	82
Salt Lake City, UT	179	8.5	0.6	2.2	11	85
San Antonio, TX	126	3.9	1.1	2.3	6	60
San Diego, CA	186	7.1	1.0	0.9	8	90
San Francisco, CA	222	4.8	1.8	0.7	25	70
Tampa, FL	217	4.4	1.1	1.0	8	68
Tulsa, OK	216	5.3	0.9	1.8	15	70
Washington, DC	268	5.3	0.9	1.4	13	99

aldehydes, 1% ketones, and 2% acetylene. The detailed composition of this mixture is given elsewhere (Carter, 1993, 1994b).

Adjusted NO_x scenarios

Incremental reactivities in the base case scenarios would be expected to vary widely, since incremental reactivities depend on the ROG/NO_x ratio, and that ratio varies widely among the base case scenarios. To obtain reactivity scales for specified NO_x conditions, separate sets of scenarios, designated MIR (for maximum incremental reactivity), MOR (for maximum ozone reactivity), and Equal Benefit Incremental Reactivity (EBIR) were developed (Carter, 1984). In the MIR scenarios, the NO_x inputs were adjusted so the base ROG mixture (and most other VOCs) have their highest incremental reactivity. This is representative of the highest NO_x conditions of relevance to VOC reactivity assessment because at higher NO_x levels O_3 yields become significantly suppressed, but is also the condition where O_3 is most sensitive to VOC emissions. In the MOR scenarios, the NO_x inputs were adjusted to yield the highest ozone concentration. In the EBIR scenarios, the NO_x inputs were adjusted so that the relative effects of NO_x reductions and total ROG reductions on peak ozone levels were equal. This represents the lowest NO_x condition of relevance for VOC reactivity assessment, because O_3 formation becomes more sensitive to NO_x emissions than VOC emissions at lower NO_x levels. The changes in the base case ROG/NO_x ratios which yielded the MOR scenarios are given in Table 3. As discussed by Carter (1994a) the MIR and EBIR ROG/NO_x ratios are respectively ~1.5 and ~0.7 times those for the MOR scenarios in all cases.

For this study, the MIR, MOIR, and EBIR reactivities were calculated using the "averaged conditions" scenarios with the corresponding adjusted NO_x conditions. As discussed by Carter (1994a), averaged conditions scenarios have all inputs derived by averaging the corresponding inputs of the base case scenarios, except that the NO_x inputs were adjusted to yield the specified NO_x conditions as discussed above. This is slightly different than the approach used by Carter (1994a) to derive the MIR, MOIR, and EBIR scales, which involved adjusting NO_x conditions separately for each of the 39 base case scenarios, and then averaging the reactivities derived from them. Since Carter (1994a) showed that both approaches yield essentially the same result, for this work use of the averaged conditions approach was preferred because it is computationally much more straightforward, and gives an equally good indication of how the relative reactivities of compounds vary with varying NO_x conditions.

NO_x Conditions in the Base Case Scenarios

The variability of ROG/NO_x ratios in the base case scenarios suggest a variability of reactivity characteristics in the base case scenarios. However, as discussed previously (Carter, 1994a), the ROG/NO_x ratio is also variable in the MIR or MOR scenarios, despite the fact that the NO_x inputs in these scenarios are adjusted to yield a specified reactivity characteristic. Thus, the ROG/NO_x ratio, by itself, is not necessarily a good predictor of reactivity characteristics of a particular scenario. The NO_x/NO_x^{MOR} ratio is a much better predictor of this, with values greater than 1 indicating relatively high NO_x conditions where ozone formation is more sensitive to VOCs, and values less than 1 indicating NO_x-limited

conditions. NO_x/NO_x^{MOR} ratios less than 0.7 represent conditions where NO_x control is a more effective ozone control strategy than ROG control (Carter, 1994a). Note that more than half of the base case scenarios represent NO_x-limited conditions, and ~25% of them represent conditions where NO_x control is more beneficial than VOC control. A relatively small number of scenarios represent MIR or near MIR conditions. However, as discussed elsewhere (Carter, 1994a), this set of scenarios is based on near-worst-case conditions for ozone formation in each of the airsheds. Had scenarios representing less-than-worst-case conditions been included, one might expect a larger number of MIR or near MIR scenarios. This is because NO_x is consumed more slowly on days with lower light intensity or temperature, and thus the scenario is less likely to become NO_x-limited.

Incremental and Relative Reactivities

The incremental reactivity of a VOC in an airshed scenario is the change in ozone caused by adding the VOC to the emissions, divided by the amount of VOC added, calculated for sufficiently small amounts of added VOC that the incremental reactivity is independent of the amount added. The procedure used to calculate incremental reactivities in a scenario was as discussed in detail elsewhere (Carter, 1993, 1994a,b). The incremental reactivities depend on how the amount of VOC added are quantified. In this work, the added VOC was quantified on a mass basis, since this is how VOCs are regulated. In addition, the incremental reactivities also depend on how ozone impacts are quantified (Carter, 1994a). In this work, two different ozone quantifications were used, resulting in two different incremental reactivities being calculated for a VOC in a scenario. These are discussed below.

The "Ozone Yield" incremental reactivities measure the effect of the VOC on the total amount of ozone formed in the scenario at the time of its maximum concentration. In this work, this is quantified as grams O_3 formed per gram VOC added. This gives the same ratios of incremental reactivities as reactivities calculated from peak ozone concentrations, but is preferred because it permits magnitudes of reactivities in scenarios with differing dilutions to be compared on the same basis. Most previous recent studies of incremental reactivity (Dodge, 1984; Carter and Atkinson, 1987, 1989a, Chang and Rudy, 1990; Jeffries and Crouse, 1991) have all been based on ozone yield or peak ozone concentration reactivities.

The ozone yield incremental reactivities do not necessarily measure the effect of the VOC on exposure to unacceptable levels of ozone because it does not measure how long high levels of ozone are present. A quantification which reflects this is integrated ozone over the standard, which is defined as the sum of the hourly ozone concentrations for the hours when ozone exceeds the standard in the base case scenarios (Carter 1994a). In the previous work (Carter, 1994a), we used the California ozone standard of 90 ppb, but in this work we will use the national standard of 0.12 ppm. Reactivities relative to this quantification of ozone are referred to by the abbreviation "$IntO_3$>0.12" reactivities.

Relative reactivities are ratios of incremental reactivities to incremental reactivities of some standard VOC or mixture. Since these are the quantities which usually are the most relevant to control

strategy applications, the results in this work will be given in terms of relative reactivities. In our previous work (Carter 1991, 1994a), we used the incremental reactivity of the base ROG mixture, i.e., the mixture representing ROG pollutants from all sources, as the standard to define relative reactivities. However, because of the tendency within the EPA to consider ethane as the standard to define exempt vs controlled VOCs, in this work we will present reactivity ratios where ethane is used as the standard.

Reactivity Scales

A reactivity scale is a set of incremental or relative reactivities for a particular scenario or group of scenarios. Two types of reactivity scales will be discussed here, "base case" scales and adjusted NO_x scales. Base case scales are simply the set of incremental or relative reactivities in the 39 base case scenarios. Two sets of base case scales are derived — those based on ozone yield reactivities and those based on $IntO_3$>0.12 reactivities. In the previous work (Carter, 1991, 1994a) we derived various multi-scenario scales from the individual base case scales by averaging or other procedures, to evaluate alternative approaches for developing single reactivity scales for applications requiring single scales. However, the decision of whether to exempt a VOC should not be made based on relative reactivities of a single scale, but on a knowledge of the range of relative reactivities for a variety of conditions. Thus in this work we present the distribution of base case relative reactivities for the 39 individual scenarios rather than developing aggregated or optimum scales which represent the distribution by single numbers.

The adjusted NO_x incremental reactivity scales refer to the MIR (maximum incremental reactivity), MOIR (maximum ozone incremental reactivity), or the EBIR (Equal Benefit Incremental Reactivity) scales. In this work, these consist of ozone yield incremental reactivities in averaged conditions scenarios where NO_x inputs were adjusted to yield MIR, MOR or EBIR conditions, respectively. Relative reactivities in these scales are ratios of incremental reactivities in these scales. Reactivities in the MIR scale are of interest because the California Air Resources Board utilized an MIR scale to calculate reactivity adjustment factors in its clean fuels/low emissions vehicle regulations (CARB, 1993). The justification for using this scale in applications requiring a single scale (such as the CARB vehicle regulations) is that it reflects conditions where ozone is most sensitive to changes in VOC emissions, and complements NO_x control, which is most effective for reducing ozone under conditions where the MIR scale is least applicable (Carter, 1994a). The MOIR scale is preferred by many as an alternative for such applications because it reflects conditions which are most favorable for ozone, and is more representative of the distribution of conditions in the base case scenarios (Carter 1994a). Most other alternative reactivity scales which might be appropriate for assessing VOC control strategies (i.e., excluding scales representing highly NO_x-limited conditions where ozone is more sensitive to NO_x than VOCs) tend to fall in the range defined by the MIR and MOIR scales. Since the EBIR scale represents lower NO_x conditions where O_3 is less sensitive to VOCs, its use in applications requiring a single scale has not been considered. However, it is useful for assessing how reactivities depend on NO_x conditions.

Note that the MIR, MOIR, EBIR and base case scales derived in this work are somewhat different from those calculated previously (Carter, 1994a; Carter et al, 1993b) because an updated chemical mechanism was used. The updates to the mechanism were discussed in the previous section. In addition, as indicated above, for computational efficiency the MIR, MOIR and EBIR scales were calculated using a single averaged conditions scenario, rather than the average of the adjusted NO_x base case scenarios as done previously (Carter, 1994a).

Calculated Relative Reactivities of Propylene Glycol

Table 4 lists, for the base case and the adjusted NO_x averaged conditions scenarios, the ozone yield and $IntO_3$>0.12 reactivities of PG, ethane, and several other representative VOCs relative to the total of all emitted VOCs. Unlike some VOCs, such as toluene, PG's relative reactivities are not highly variable from scenario to scenario, though its ozone yield relative reactivity tends to increase somewhat in the lower NO_x scenarios. It can be seen that propylene glycol is calculated to form considerably more ozone than ethane, and thus would be unlikely to be a reasonable candidate for exemption under the criteria presently used by the EPA. On the other hand, it is clear that PG is not reasonably categorized as a "high reactivity" compound, having a lower MIR and integrated ozone reactivities than toluene and the total of all emitted VOCs, and approximately the same ozone yield reactivity as the total of emitted VOCs for the base case scenario. It has less than half the ozone impact as m-xylene, which is an example of a high reactivity VOC. Overall, these calculations indicate that the ozone impact of PG is comparable to or somewhat less than the average of all emitted VOCs.

Note that the PG reactivity estimates shown on Table 4 were calculated using the OH + PG rate constant of Aschmann and Atkinson (1997). The results of the higher NO_x PG reactivity experiments are slightly more consistent with predictions of the model using an OH + PG rate constant which is ~25% higher. To assess whether this has a significant effect on these relative reactivity predictions, reactivities for the three averaged conditions scenarios were also calculated using the ~25% higher OH + PG rate constant derived from the relative PG consumption rates in our experiments. This yielded relative ozone yield reactivities which were only 6-7% higher than those calculated using the Aschmann and Atkinson (1997) rate constant, and relative integrated ozone reactivities which were only 8% higher. This difference is clearly not a significant factor affecting the overall conclusions of the study concerning the atmospheric ozone impact of PG.

Table 4. Summary of calculated relative incremental reactivities (gram basis) for selected VOCs comppared to those for the total of all emitted VOCs.

Scenario	Relative to the Total of Emitted VOCS (Base ROG)							
	O_3 Yield Reactivity				$IntO_3$ >0.12 Reactivity			
	Ethane	Pr.Glycol	Toluene	m-Xylene	Ethane	Pr.Glycol	Toluene	m-Xylene
Averaged Conditions								
Max React	0.08	0.59	1.25	3.5	0.07	0.57	1.18	3.5
Max Ozone	0.15	0.81	0.83	2.7	0.10	0.64	0.99	3.2
Equal Benefit	0.19	1.00	0.18	2.3	0.12	0.76	0.54	2.9
Base Case								
Average	**0.17**	**0.94**	**0.40**	**2.4**	**0.11**	**0.73**	**0.71**	**3.0**
St.Dev	**23%**	**18%**	**153%**	**16%**	**25%**	**18%**	**43%**	**10%**
ATL GA	0.17	0.91	0.66	2.5	0.12	0.74	0.78	2.9
AUS TX	0.19	1.08	0.21	2.2	0.14	0.88	0.38	2.5
BAL MD	0.15	0.90	0.56	2.5	0.09	0.64	0.91	3.3
BAT LA	0.15	0.78	0.71	2.7	0.10	0.63	0.87	3.2
BIR AL	0.23	1.22	-0.31	1.8	0.13	0.84	0.35	2.8
BOS MA	0.20	1.01	0.37	2.0	0.12	0.76	0.66	2.7
CHA NC	0.20	1.18	0.20	2.1	0.16	1.04	0.34	2.4
CHI IL	0.27	1.42	-2.02	1.7	0.14	0.89	-0.40	2.7
CIN OH	0.19	1.03	0.43	2.1	0.12	0.77	0.75	2.8
CLE OH	0.15	0.85	0.53	2.6	0.09	0.62	0.86	3.2
DAL TX	0.12	0.70	1.20	3.1	0.09	0.59	1.15	3.4
DEN CO	0.11	0.71	0.80	3.0	0.07	0.56	0.99	3.5
DET MI	0.20	1.02	0.33	2.1	0.11	0.72	0.77	3.0
ELP TX	0.11	0.75	0.88	3.1	0.08	0.59	0.99	3.5
HAR CT	0.20	1.10	0.26	2.1	0.15	0.89	0.54	2.7
HOU TX	0.18	0.91	0.51	2.3	0.11	0.68	0.79	3.1
IND IN	0.16	0.85	0.69	2.7	0.11	0.66	0.94	3.2
JAC FL	0.16	0.87	0.65	2.6	0.13	0.77	0.71	2.9
KAN MO	0.19	1.04	0.56	2.1	0.14	0.85	0.74	2.7
LAK LA	0.22	0.97	-0.06	2.3	0.14	0.72	0.37	3.1
LOS CA	0.15	0.90	-0.16	2.5	0.08	0.62	0.56	3.4
LOU KY	0.19	0.88	0.75	2.4	0.13	0.73	0.89	2.8
MEM TN	0.20	1.00	0.28	2.2	0.13	0.77	0.60	2.9
MIA FL	0.18	1.08	0.27	2.5	0.17	1.05	0.30	2.6
NAS TN	0.23	1.15	0.28	2.1	0.19	1.05	0.39	2.4
NEW NY	0.17	0.95	-1.52	2.0	0.09	0.64	0.12	2.9
PHI PA	0.17	0.88	0.59	2.5	0.11	0.69	0.85	3.0
PHO AZ	0.16	0.98	0.39	2.5	0.09	0.68	0.82	3.3
POR OR	0.17	0.92	0.70	2.5	0.14	0.80	0.80	2.8
RIC VA	0.18	1.03	0.32	2.2	0.12	0.75	0.72	2.9
SAC CA	0.17	0.91	0.78	2.6	0.12	0.73	0.97	3.2
SAI MO	0.14	0.85	0.52	2.6	0.08	0.61	0.86	3.3
SAL UT	0.19	1.08	0.27	2.2	0.12	0.79	0.65	3.0
SAN TX	0.13	0.75	1.17	2.9	0.12	0.72	1.16	3.0
SDO CA	0.12	0.74	0.65	2.9	0.09	0.64	0.83	3.3
SFO CA	0.05	0.52	1.15	3.7	0.05	0.50	1.08	3.8
TAM FL	0.13	0.72	0.98	2.9	0.09	0.59	1.06	3.4
TUL OK	0.18	0.90	0.64	2.3	0.11	0.69	0.89	3.0
WAS DC	0.19	0.98	0.36	2.2	0.11	0.70	0.72	3.0

CONCLUSIONS

A quantitative evaluation of how emissions of a compound affects air quality requires developing a chemical mechanism for the compound's atmospheric reactions which can be reliably used in airshed models to predict its atmospheric ozone impacts under a variety of conditions. Until this study, there was no information concerning the effects of PG on ozone formation, or to test the accuracy of model predictions of these effects. The objective of this study was to provide the data needed for this purpose, and obtain more reliable atmospheric ozone impacts for this compound. We feel that this program achieved this objective.

The rate of consumption of PG in our chamber experiments could be used to derive an OH + PG rate constant of (2.8±0.3) x 10^{-11} cm^3 $molec^{-1}$ s^{-1}, which is ~25% higher than, but within experimental uncertainty of, the value of (2.2±0.1) x 10^{-11} cm^3 $molec^{-1}$ s^{-1} recently obtained by Aschmann and Atkinson (1997) using a similar, but somewhat more precise, relative rate method. These are around a factor of two higher than the previously measured OH + PG rate constant, which probably was affected by wall absorption problems and now appears to be incorrect. The more precise Aschmann and Atkinson (1997) rate constant is considered more appropriate for use in atmospheric reactivity simulations.

Model predictions using the recently determined OH + PG rate constants and an estimated mechanism for its subsequent reactions are found to be consistent, to within experimental uncertainty, with the effects of PG on NO oxidation, O_3 formation, and OH radical levels observed in the environmental chamber experiments. The data are slightly better fit using the ~25% higher rate constant derived from the PG consumption rate in our chamber data than that derived from the more precise relative measurement of Aschmann and Atkinson, but the differences were found to have less than a 10% impact on atmospheric ozone calculations. Although the product yield estimates for the overall OH + PG process are somewhat uncertain, results of model simulations were not sensitive to this uncertainty. We conclude that the OH + PG mechanism is sufficiently well established to be used for the purpose of estimating the effects of PG on ozone formation in the atmosphere.

When applied to atmospheric ozone impact simulations, the model predicted that PG has a comparable, though slightly smaller, impact on ozone formation as an equal mass as the average of emissions from all sources. This would mean that PG does not have sufficiently low reactivity to be appropriate for exemption from regulation as a VOC ozone precursor under the criteria presently used by the EPA. However, it can also be concluded that it is not appropriate that PG be categorized as highly reactive, since these results indicate that regulating emissions of PG is slightly less effective in reducing ozone as regulating emissions of all other VOCs equally, under most atmospheric conditions.

REFERENCES

Aschmann, S. A. and R. Atkinson (1997): Statewide Air Pollution Research Center, University of California, Riverside. Data to be submitted for publication.

Atkinson, R. (1987): "A Structure-Activity Relationship for the Estimation of Rate Constants for the Gas-Phase Reactions of OH Radicals with Organic Compounds," Int. J. Chem. Kinet., 19, 799-828.

Atkinson, R. (1989): "Kinetics and Mechanisms of the Gas-Phase Reactions of the Hydroxyl Radical with Organic Compounds," J. Phys. Chem. Ref. Data, Monograph no 1.

Atkinson, R. (1991): "Kinetics and Mechanisms of the Gas-Phase Reactions of the NO_3 Radical with Organic Compounds," J. Phys. Chem. Ref. Data, 20, 459-507.

Atkinson, R. (1997): "Gas-Phase Tropospheric Chemistry of Volatile Organic Compounds: 1. Alkanes and Alkenes," J. Phys. Chem. Ref. Data, in press.

Atkinson, R. and W. P. L. Carter (1984): "Kinetics and Mechanisms of the Gas-Phase Reactions of Ozone with Organic Compounds under Atmospheric Conditions," Chem. Rev. 1984, 437-470.

Baugues, K. (1990): "Preliminary Planning Information for Updating the Ozone Regulatory Impact Analysis Version of EKMA," Draft Document, Source Receptor Analysis Branch, Technical Support Division, U. S. Environmental Protection Agency, Research Triangle Park, NC, January.

Campbell, I. M. and P. E. Parkinson (1978): Chem. Phys. Lett. 53, 385.

CARB (1993): "Proposed Regulations for Low-Emission Vehicles and Clean Fuels — Staff Report and Technical Support Document," California Air Resources Board, Sacramento, CA, August 13, 1990. See also Appendix VIII of "California Exhaust Emission Standards and Test Procedures for 1988 and Subsequent Model Passenger Cars, Light Duty Trucks and Medium Duty Vehicles," as last amended September 22, 1993. Incorporated by reference in Section 1960.1 (k) of Title 13, California Code of Regulations.

Carter, W. P. L. (1990): "A Detailed Mechanism for the Gas-Phase Atmospheric Reactions of Organic Compounds," Atmos. Environ., 24A, 481-518.

Carter, W. P. L. (1991): "Development of Ozone Reactivity Scales for Volatile Organic Compounds", EPA-600/3-91/050, August.

Carter, W. P. L. (1993): "Development and Application of an Up-To-Date Photochemical Mechanism for Airshed Modeling and Reactivity Assessment," Draft final report for California Air Resources Board Contract No. A934-094, April 26.

Carter, W. P. L. (1994a): "Development of Ozone Reactivity Scales for Volatile Organic Compounds," J. Air & Waste Manage. Assoc., 44, 881-899.

Carter, W. P. L. (1994b): "Calculation of Reactivity Scales Using an Updated Carbon Bond IV Mechanism," Draft Report Prepared for Systems Applications International Under Funding from the Auto/Oil Air Quality Improvement Research Program, April 12.

Carter, W. P. L. (1995): "Computer Modeling of Environmental Chamber Measurements of Maximum Incremental Reactivities of Volatile Organic Compounds," Atmos. Environ., 29, 2513-2517.

Carter, W. P. L. and R. Atkinson (1987): "An Experimental Study of Incremental Hydrocarbon Reactivity," Environ. Sci. Technol., 21, 670-679

Carter, W. P. L. and R. Atkinson (1989a): "A Computer Modeling Study of Incremental Hydrocarbon Reactivity", Environ. Sci. Technol., 23, 864.

Carter, W. P. L. and R. Atkinson (1989b): "Alkyl Nitrate Formation from the Atmospheric Photooxidation of Alkanes; a Revised Estimation Method," J. Atm. Chem. 8, 165-173.

Carter, W. P. L., and F. W. Lurmann (1990): "Evaluation of the RADM Gas-Phase Chemical Mechanism," Final Report, EPA-600/3-90-001.

Carter, W. P. L. and F. W. Lurmann (1991): "Evaluation of a Detailed Gas-Phase Atmospheric Reaction Mechanism using Environmental Chamber Data," Atm. Environ. 25A, 2771-2806.

Carter, W. P. L., J. A. Pierce, I. L. Malkina, D. Luo and W. D. Long (1993a): "Environmental Chamber Studies of Maximum Incremental Reactivities of Volatile Organic Compounds," Report to Coordinating Research Council, Project No. ME-9, California Air Resources Board Contract No. A032-0692; South Coast Air Quality Management District Contract No. C91323, United States Environmental Protection Agency Cooperative Agreement No. CR-814396-01-0, University Corporation for Atmospheric Research Contract No. 59166, and Dow Corning Corporation. April 1.

Carter, W. P. L, D. Luo, I. L. Malkina, and J. A. Pierce (1993b): "An Experimental and Modeling Study of the Photochemical Ozone Reactivity of Acetone," Final Report to Chemical Manufacturers Association Contract No. KET-ACE-CRC-2.0. December 10.

Carter, W. P. L., D. Luo, I. L. Malkina, and J. A. Pierce (1995a): "Environmental Chamber Studies of Atmospheric Reactivities of Volatile Organic Compounds. Effects of Varying ROG Surrogate and NO_x," Final report to Coordinating Research Council, Inc., Project ME-9, California Air Resources Board, Contract A032-0692, and South Coast Air Quality Management District, Contract C91323. March 24.

Carter, W. P. L., D. Luo, I. L. Malkina, and D. Fitz (1995b): "The University of California, Riverside Environmental Chamber Data Base for Evaluating Oxidant Mechanism. Indoor Chamber Experiments through 1993," Report submitted to the U. S. Environmental Protection Agency, EPA/AREAL, Research Triangle Park, NC., March 20..

Carter, W. P. L., J. A. Pierce, D. Luo, and I. L. Malkina (1995c): "Environmental Chamber Study of Maximum Incremental Reactivities of Volatile Organic Compounds," Atmos. Environ. 29, 2499-2511.

Carter, W. P. L., D. Luo, I. L. Malkina, and J. A. Pierce (1995d): "Environmental Chamber Studies of Atmospheric Reactivities of Volatile Organic Compounds. Effects of Varying Chamber and Light Source," Final report to National Renewable Energy Laboratory, Contract XZ-2-12075, Coordinating Research Council, Inc., Project M-9, California Air Resources Board, Contract A032-0692, and South Coast Air Quality Management District, Contract C91323, March 26.

Carter, W. P. L. and R. Atkinson (1996): "Development and Evaluation of a Detailed Mechanism for the Atmospheric Reactions of Isoprene and NO_x," Int. J. Chem. Kinet., 28, 497-530.

Carter, W. P. L., D. Luo, and I. L. Malkina (1997): "Environmental Chamber Studies for Development of an Updated Photochemical Mechanism for VOC Reactivity Assessment," Draft final report to California Air Resources Board Contract 92-345, Coordinating Research Council Project M-9, and National Renewable Energy Laboratory Contract ZF-2-12252-07. March 10.

Chang, T. Y. and S. J. Rudy (1990): "Ozone-Forming Potential of Organic Emissions from Alternative-Fueled Vehicles," Atmos. Environ., 24A, 2421-2430.

Croes, B. E., Technical Support Division, California Air Resources Board, personal communication (1991).

Croes, B. E., et al. (1994): "Southern California Air Quality Study Data Archive," Research Division, California Air Resources Board.

Dimitriades, B. (1996): "Scientific Basis for the VOC Reactivity Issues Raised by Section 183(e) of the Clean Air Act Amendments of 1990," J. Air Waste Manage. Assoc. 46, 963-970.

Dodge, M. C. (1984): "Combined effects of organic reactivity and NMHC/NOx ratio on photochemical oxidant formation -- a modeling study," Atmos. Environ., 18, 1657.

EPA (1984): "Guideline for Using the Carbon Bond Mechanism in City-Specific EKMA," EPA-450/4-84-005, February.

Gery, M. W., R. D. Edmond and G. Z. Whitten (1987): "Tropospheric Ultraviolet Radiation. Assessment of Existing Data and Effects on Ozone Formation," Final Report, EPA-600/3-87-047, October.

Gipson, G. L., W. P. Freas, R. A. Kelly and E. L. Meyer, "Guideline for Use of City-Specific EKMA in Preparing Ozone SIPs, EPA-450/4-80-027, March, 1981.

Gipson, G. L. and W. P. Freas (1983): "Use of City-Specific EKMA in the Ozone RIA," U. S. Environmental Protection Agency, July.

Gipson, G. L. (1984): "Users Manual for OZIPM-2: Ozone Isopleth Plotting Package With Optional Mechanism/Version 2," EPA-450/4-84-024, August.

Hogo, H. and M. W. Gery (1988): "Guidelines for Using OZIPM-4 with CBM-IV or Optional Mechanisms. Volume 1. Description of the Ozone Isopleth Plotting Package Version 4", Final Report for EPA Contract No. 68-02-4136, Atmospheric Sciences Research Laboratory, Research Triangle Park, NC. January.

Jeffries, H. E., K. G. Sexton, J. R. Arnold, and T. L. Kale (1989): "Validation Testing of New Mechanisms with Outdoor Chamber Data. Volume 2: Analysis of VOC Data for the CB4 and CAL Photochemical Mechanisms," Final Report, EPA-600/3-89-010b.

Jeffries, H. E. and R. Crouse (1991): "Scientific and Technical Issues Related to the Application of Incremental Reactivity. Part II: Explaining Mechanism Differences," Report prepared for Western States Petroleum Association, Glendale, CA, October.

Jeffries, H. E. (1991): "UNC Solar Radiation Models," unpublished draft report for EPA Cooperative Agreements CR813107, CR813964 and CR815779". Undated.

Johnson, G. M. (1983): "Factors Affecting Oxidant Formation in Sydney Air," in "The Urban Atmosphere -- Sydney, a Case Study." Eds. J. N. Carras and G. M. Johnson (CSIRO, Melbourne), pp. 393-408.

Kwok, E. S. C., and R. Atkinson (1995): "Estimation of Hydroxyl Radical Reaction Rate Constants for Gas-Phase Organic Compounds Using a Structure-Reactivity Relationship: An Update," Atmos. Environ 29, 1685-1695.

Lurmann, F. W. and H. H. Main (1992): "Analysis of the Ambient VOC Data Collected in the Southern California Air Quality Study," Final Report to California Air Resources Board Contract No. A832-130, February.

Pitts, J. N., Jr., E. Sanhueza, R. Atkinson, W. P. L. Carter, A. M. Winer, G. W. Harris, and C. N. Plum (1984): "An Investigation of the Dark Formation of Nitrous Acid in Environmental Chambers," Int. J. Chem. Kinet., 16, 919-939.

Tuazon, E. C., R. Atkinson, C. N. Plum, A. M. Winer, and J. N. Pitts, Jr. (1983): "The Reaction of Gas-Phase N_2O_5 with Water Vapor," Geophys. Res. Lett. 10, 953-956.

Tuazon, E. C., W. P. L. Carter, R. Atkinson, and J. N. Pitts, Jr. (1983): The Gas-Phase Reaction of Hydrazine and Ozone: A Non-Photolytic Source for Measurement of Relative OH Radical Rate Constants," Int. J. Chem. Kinetic., 15, 619-629.

Wiedelmann, A., and C. Zetzch (1982): Presented at Bunsentagung, Ulm and Neu-Ulm, May 20-22.

Zafonte, L., P. L. Rieger, and J. R. Holmes (1977): "Nitrogen Dioxide Photolysis in the Los Angeles Atmosphere," Environ. Sci. Technol. 11, 483-487.

APPENDIX A
LISTING OF THE CHEMICAL MECHANISM

The chemical mechanism used in the environmental chamber and atmospheric model simulations discussed in this report is given in Tables A-1 through A-4. Table A-1 lists the species used in the mechanism, Table A-2 gives the reactions and rate constants, Table A-3 gives the parameters used to calculate the rates of the photolysis reactions, and Table A-4 gives the values and derivations of the chamber-dependent parameters used when modeling the environmental chamber experiments. Footnotes to Table A-2 indicate the format used for the reaction listing.

Table A-1. List of species in the chemical mechanism used in the model simulations for this study.

Name	Description
Constant Species.	
O2	Oxygen
M	Air
H2O	Water
Active Inorganic Species.	
O3	Ozone
NO	Nitric Oxide
NO2	Nitrogen Dioxide
NO3	Nitrate Radical
N2O5	Nitrogen Pentoxide
HONO	Nitrous Acid
HNO3	Nitric Acid
HNO4	Peroxynitric Acid
HO2H	Hydrogen Peroxide
Active Radical Species and Operators.	
HO2.	Hydroperoxide Radicals
RO2.	Operator to Calculate Total Organic Peroxy Radicals
RCO3.	Operator to Calculate Total Acetyl Peroxy Radicals
Active Reactive Organic Product Species.	
CO	Carbon Monoxide
HCHO	Formaldehyde
CCHO	Acetaldehyde
RCHO	Lumped C3+ Aldehydes
ACET	Acetone
MEK	Lumped Ketones
PHEN	Phenol
CRES	Cresols
BALD	Aromatic aldehydes (e.g., benzaldehyde)

Table A-1, (continued)

Name	Description
GLY	Glyoxal
MGLY	Methyl Glyoxal
AFG1	Reactive Aromatic Fragmentation Products from benzene and naphthalene
AFG2	Other Reactive Aromatic Fragmentation Products
AFG3	Aromatic Fragmentation Products used in adjusted m-xylene mechanism
RNO3	Organic Nitrates
NPHE	Nitrophenols
ISOPROD	Lumped isoprene product species
PAN	Peroxy Acetyl Nitrate
PPN	Peroxy Propionyl Nitrate
GPAN	PAN Analogue formed from Glyoxal
PBZN	PAN Analogues formed from Aromatic Aldehydes
-OOH	Operator Representing Hydroperoxy Groups
Non-Reacting Species	
CO2	Carbon Dioxide
-C	"Lost Carbon"
-N	"Lost Nitrogen"
H2	Hydrogen
Steady State Species and Operators.	
HO.	Hydroxyl Radicals
O	Ground State Oxygen Atoms
O*1D2	Excited Oxygen Atoms
RO2-R.	Peroxy Radical Operator representing NO to NO_2 conversion with HO_2 formation.
RO2-N.	Peroxy Radical Operator representing NO consumption with organic nitrate formation.
RO2-NP.	Peroxy Radical Operator representing NO consumption with nitrophenol formation
R2O2.	Peroxy Radical Operator representing NO to NO_2 conversion.
CCO-O2.	Peroxy Acetyl Radicals
C2CO-O2.	Peroxy Propionyl Radicals
HCOCO-O2.	Peroxyacyl Radical formed from Glyoxal
BZ-CO-O2.	Peroxyacyl Radical formed from Aromatic Aldehydes
HOCOO.	Intermediate formed in Formaldehyde + HO_2 reaction
BZ-O.	Phenoxy Radicals
BZ(NO2)-O.	Nitratophenoxy Radicals
HOCOO.	Radical Intermediate formed in the HO_2 + Formaldehyde system.
(HCHO2)	Excited Criegee biradicals formed from $=CH_2$ groups
(CCHO2)	Excited Criegee biradicals formed from $=CHCH_3$ groups
(RCHO2)	Excited Criegee biradicals formed from =CHR groups, where R not CH_3
(C(C)CO2)	Excited Criegee biradicals formed from $=C(CH_3)_2$ groups
(C(R)CO2)	Excited Criegee biradicals formed from $=C(CH_3)R$ or CR_2 groups
(BZCHO2)	Excited Criegee biradicals formed from styrenes
Hydrocarbon species represented explicitly	
CH4	Methane (EKMA simulations only)
ETHANE	Ethane (Ethane reactivity simulations only)
N-C4	n-Butane (Chamber simulations only)
N-C6	n-Hexane (Chamber simulations only)
N-C8	n-Octane (Chamber simulations only)
ETHE	Ethene

Table A-1, (continued)

Name	Description
ISOP	Isoprene (EKMA Simulations only)
APIN	α-Pinene (EKMA Simulations only)
UNKN	Unknown biogenics. (EKMA Simulations only)
PROPENE	Propene (Chamber simulations only)
T-2-BUTE	trans-2-Butene (Chamber simulations only)
TOLUENE	Toluene
M-XYLENE	m-Xylene
PR-GLYCL	Propylene glycol
Lumped species used to represent the Base ROG mixture in the EKMA model simulations.	
ALK1	Alkanes and other saturated compounds with $k_{OH} < 10^4$ ppm^{-1} min^{-1}.
ALK2	Alkanes and other saturated compounds with $k_{OH} \geq 10^4$ ppm^{-1} min^{-1}.
ARO1	Aromatics with $k_{OH} < 2x10^4$ ppm^{-1} min^{-1}.
ARO2	Aromatics with $k_{OH} \geq 2x10^4$ ppm^{-1} min^{-1}.
OLE1	Alkenes (other than ethene) with $k_{OH} < 7x10^4$ ppm^{-1} min^{-1}.
OLE2	Alkenes with $k_{OH} \geq 7x10^4$ ppm^{-1} min^{-1}.

Table A-2. List of reactions in the chemical mechanism used in the model simulations for this study.

Rxn. Label	Kinetic Parameters [a] k(300)	A	Ea	B	Reactions [b]
Inorganic Reactions					
1	(Phot. Set = NO2)				NO2 + HV = NO + O
2	6.00E-34	6.00E-34	0.00	-2.30	O + O2 + M = O3 + M
3A	9.69E-12	6.50E-12	-0.24	0.00	O + NO2 = NO + O2
3B	1.55E-12	(Falloff Kinetics)			O + NO2 = NO3 + M
	k0 =	9.00E-32	0.00	-2.00	
	kINF =	2.20E-11	0.00	0.00	
		F= 0.60	n= 1.00		
4	1.88E-14	2.00E-12	2.78	0.00	O3 + NO = NO2 + O2
5	3.36E-17	1.40E-13	4.97	0.00	O3 + NO2 = O2 + NO3
6	2.80E-11	1.70E-11	-0.30	0.00	NO + NO3 = 2 NO2
7	1.92E-38	3.30E-39	-1.05	0.00	NO + NO + O2 = 2 NO2
8	1.26E-12	(Falloff Kinetics)			NO2 + NO3 = N2O5
	k0 =	2.20E-30	0.00	-4.30	
	kINF =	1.50E-12	0.00	-0.50	
		F= 0.60	n= 1.00		
9	5.53E+10	9.09E+26	22.26	0.00	N2O5 + #RCON8 = NO2 + NO3
10	1.00E-21	(No T Dependence)			N2O5 + H2O = 2 HNO3
11	4.17E-16	2.50E-14	2.44	0.00	NO2 + NO3 = NO + NO2 + O2
12A	(Phot. Set = NO3NO)				NO3 + HV = NO + O2
12B	(Phot. Set = NO3NO2)				NO3 + HV = NO2 + O
13A	(Phot. Set = O3O3P)				O3 + HV = O + O2
13B	(Phot. Set = O3O1D)				O3 + HV = O*1D2 + O2
14	2.20E-10	(No T Dependence)			O*1D2 + H2O = 2 HO.
15	2.92E-11	1.92E-11	-0.25	0.00	O*1D2 + M = O + M
16	4.81E-12	(Falloff Kinetics)			HO. + NO = HONO
	k0 =	7.00E-31	0.00	-2.60	
	kINF =	1.50E-11	0.00	-0.50	
		F= 0.60	n= 1.00		
17	(Phot. Set = HONO)				HONO + HV = HO. + NO
18	1.13E-11	(Falloff Kinetics)			HO. + NO2 = HNO3
	k0 =	2.60E-30	0.00	-3.20	
	kINF =	2.40E-11	0.00	-1.30	
		F= 0.60	n= 1.00		
19	1.03E-13	6.45E-15	-1.65	0.00	HO. + HNO3 = H2O + NO3
21	2.40E-13	(No T Dependence)			HO. + CO = HO2. + CO2
22	6.95E-14	1.60E-12	1.87	0.00	HO. + O3 = HO2. + O2
23	8.28E-12	3.70E-12	-0.48	0.00	HO2. + NO = HO. + NO2
24	1.37E-12	(Falloff Kinetics)			HO2. + NO2 = HNO4
	k0 =	1.80E-31	0.00	-3.20	
	kINF =	4.70E-12	0.00	-1.40	
		F= 0.60	n= 1.00		
25	7.92E+10	4.76E+26	21.66	0.00	HNO4 + #RCON24 = HO2. + NO2
27	4.61E-12	1.30E-12	-0.75	0.00	HNO4 + HO. = H2O + NO2 + O2
28	2.08E-15	1.10E-14	0.99	0.00	HO2. + O3 = HO. + 2 O2
29A	1.73E-12	2.20E-13	-1.23	0.00	HO2. + HO2. = HO2H + O2
29B	5.00E-32	1.90E-33	-1.95	0.00	HO2. + HO2. + M = HO2H + O2
29C	3.72E-30	3.10E-34	-5.60	0.00	HO2. + HO2. + H2O = HO2H + O2 + H2O
29D	2.65E-30	6.60E-35	-6.32	0.00	HO2. + HO2. + H2O = HO2H + O2 + H2O
30A	1.73E-12	2.20E-13	-1.23	0.00	NO3 + HO2. = HNO3 + O2
30B	5.00E-32	1.90E-33	-1.95	0.00	NO3 + HO2. + M = HNO3 + O2
30C	3.72E-30	3.10E-34	-5.60	0.00	NO3 + HO2. + H2O = HNO3 + O2 + H2O
30D	2.65E-30	6.60E-35	-6.32	0.00	NO3 + HO2. + H2O = HNO3 + O2 + H2O
31	(Phot. Set = H2O2)				HO2H + HV = 2 HO.
32	1.70E-12	3.30E-12	0.40	0.00	HO2H + HO. = HO2. + H2O
33	9.90E-11	4.60E-11	-0.46	0.00	HO. + HO2. = H2O + O2
Peroxy Radical Operators					
B1	7.68E-12	4.20E-12	-0.36	0.00	RO2. + NO = NO
B2	2.25E-11	(Falloff Kinetics)			RCO3. + NO = NO
	k0 =	5.65E-28	0.00	-7.10	
	kINF =	2.64E-11	0.00	-0.90	
		F= 0.27	n= 1.00		
B4	1.04E-11	(Falloff Kinetics)			RCO3. + NO2 = NO2
	k0 =	2.57E-28	0.00	-7.10	
	kINF =	1.20E-11	0.00	-0.90	
		F= 0.30	n= 1.00		
B5	4.90E-12	3.40E-13	-1.59	0.00	RO2. + HO2. = HO2. + RO2-HO2-PROD
B6	4.90E-12	3.40E-13	-1.59	0.00	RCO3. + HO2. = HO2. + RO2-HO2-PROD
B8	1.00E-15	(No T Dependence)			RO2. + RO2. = RO2-RO2-PROD
B9	1.09E-11	1.86E-12	-1.05	0.00	RO2. + RCO3. = RO2-RO2-PROD
B10	1.64E-11	2.80E-12	-1.05	0.00	RCO3. + RCO3. = RO2-RO2-PROD

Table A-2 (continued)

Rxn. Label	Kinetic Parameters [a] k(300)	A	Ea	B	Reactions [b]
B11	(Same k as for RO2.)				RO2-R. + NO = NO2 + HO2.
B12	(Same k as for RO2.)				RO2-R. + HO2. = -OOH
B13	(Same k as for RO2.)				RO2-R. + RO2. = RO2. + 0.5 HO2.
B14	(Same k as for RO2.)				RO2-R. + RCO3. = RCO3. + 0.5 HO2.
B19	(Same k as for RO2.)				RO2-N. + NO = RNO3
B20	(Same k as for RO2.)				RO2-N. + HO2. = -OOH + MEK + 1.5 -C
B21	(Same k as for RO2.)				RO2-N. + RO2. = RO2. + 0.5 HO2. + MEK + 1.5 -C
B22	(Same k as for RO2.)				RO2-N. + RCO3. = RCO3. + 0.5 HO2. + MEK + 1.5 -C
B15	(Same k as for RO2.)				R2O2. + NO = NO2
B16	(Same k as for RO2.)				R2O2. + HO2. =
B17	(Same k as for RO2.)				R2O2. + RO2. = RO2.
B18	(Same k as for RO2.)				R2O2. + RCO3. = RCO3.
B23	(Same k as for RO2.)				RO2-XN. + NO = -N
B24	(Same k as for RO2.)				RO2-XN. + HO2. = -OOH
B25	(Same k as for RO2.)				RO2-XN. + RO2. = RO2. + 0.5 HO2.
B26	(Same k as for RO2.)				RO2-XN. + RCO3. = RCO3. + HO2.
G2	(Same k as for RO2.)				RO2-NP. + NO = NPHE
G3	(Same k as for RO2.)				RO2-NP. + HO2. = -OOH + 6 -C
G4	(Same k as for RO2.)				RO2-NP. + RO2. = RO2. + 0.5 HO2. + 6 -C
G5	(Same k as for RO2.)				RO2-NP. + RCO3. = RCO3. + HO2. + 6 -C
Excited Criegee Biradicals					
RZ1	(fast)				(HCHO2) = 0.7 HCOOH + 0.12 "HO. + HO2. + CO" + 0.18 "H2 + CO2"
RZ2	(fast)				(CCHO2) = 0.25 CCOOH + 0.15 "CH4 + CO2" + 0.6 HO. + 0.3 "CCO-O2. + RCO3." + 0.3 "RO2-R. + HCHO + CO + RO2."
RZ3	(fast)				(RCHO2) = 0.25 CCOOH + 0.15 CO2 + 0.6 HO. + 0.3 "C2CO-O2. + RCO3." + 0.3 "RO2-R. + CCHO + CO + RO2." + 0.55 -C
RZ4	(fast)				(C(C)CO2) = HO. + R2O2. + HCHO + CCO-O2. + RCO3. + RO2.
RZ5	(fast)				(C(R)CO2) = HO. + CCO-O2. + CCHO + R2O2. + RCO3. + RO2.
RZ6	(fast)				(CYCCO2) = 0.3 "HO. + C2CO-O2. + R2O2. + RCO3. + RO2." + 0.3 RCHO + 4.2 -C
RZ8	(fast)				(BZCHO2) = 0.5 "BZ-O. + R2O2. + CO + HO."
ISZ1	(fast)				(C:CC(C)O2) = HO. + R2O2. + HCHO + C2CO-O2. + RO2. + RCO3.
ISZ2	(fast)				(C:C(C)CHO2) = 0.75 RCHO + 0.25 ISOPROD + 0.5 -C
MAZ1	(fast)				(C2(O2)CHO) = HO. + R2O2. + HCHO + HCOCO-O2. + RO2. + RCO3.
M1Z1	(fast)				(HOCCHO2) = 0.6 HO. + 0.3 "CCO-O2. + RCO3." + 0.3 "RO2-R. + HCHO + CO + RO2." + 0.8 -C
M2Z1	(fast)				(HCOCHO2) = 0.12 "HO2. + 2 CO + HO." + 0.74 -C + 0.51 "CO2 + HCHO"
M2Z2	(fast)				(C2(O2)COH) = HO. + MGLY + HO2. + R2O2. + RO2.
Organic Product Species					
B7	(Phot. Set = CO2H)				-OOH + HV = HO2. + HO.
B7A	1.81E-12	1.18E-12	-0.25	0.00	HO. + -OOH = HO.
B7B	3.71E-12	1.79E-12	-0.44	0.00	HO. + -OOH = RO2-R. + RO2.
C1	(Phot. Set = HCHONEWR)				HCHO + HV = 2 HO2. + CO
C2	(Phot. Set = HCHONEWM)				HCHO + HV = H2 + CO
C3	9.76E-12	1.13E-12	-1.29	2.00	HCHO + HO. = HO2. + CO + H2O
C4	7.79E-14	9.70E-15	-1.24	0.00	HCHO + HO2. = HOCOO.
C4A	1.77E+02	2.40E+12	13.91	0.00	HOCOO. = HO2. + HCHO
C4B	(Same k as for RO2.)				HOCOO. + NO = -C + NO2 + HO2.
C9	6.38E-16	2.80E-12	5.00	0.00	HCHO + NO3 = HNO3 + HO2. + CO
C10	1.57E-11	5.55E-12	-0.62	0.00	CCHO + HO. = CCO-O2. + H2O + RCO3.
C11A	(Phot. Set = CCHOR)				CCHO + HV = CO + HO2. + HCHO + RO2-R. + RO2.
C12	2.84E-15	1.40E-12	3.70	0.00	CCHO + NO3 = HNO3 + CCO-O2. + RCO3.
C25	1.97E-11	8.50E-12	-0.50	0.00	RCHO + HO. = C2CO-O2. + RCO3.
C26	(Phot. Set = RCHO)				RCHO + HV = CCHO + RO2-R. + RO2. + CO + HO2.
C27	2.84E-15	1.40E-12	3.70	0.00	NO3 + RCHO = HNO3 + C2CO-O2. + RCO3.
C38	2.23E-13	4.81E-13	0.46	2.00	ACET + HO. = R2O2. + HCHO + CCO-O2. + RCO3. + RO2.
C39	(Phot. Set = ACET-93C)				ACET + HV = CCO-O2. + HCHO + RO2-R. + RCO3. + RO2.
C44	1.16E-12	2.92E-13	-0.82	2.00	MEK + HO. = H2O + 0.5 "CCHO + HCHO + CCO-O2. + C2CO-O2." + RCO3. + 1.5 "R2O2. + RO2."
C57	(Phot. Set = KETONE)				MEK + HV + #0.1 = CCO-O2. + CCHO + RO2-R. + RCO3. + RO2.

Table A-2 (continued)

Rxn. Label	Kinetic Parameters [a] k(300)	A	Ea	B	Reactions [b]
C95	2.07E-12	2.19E-11	1.41	0.00	RNO3 + HO. = NO2 + 0.155 MEK + 1.05 RCHO + 0.48 CCHO + 0.16 HCHO + 0.11 -C + 1.39 "R2O2. + RO2."
C58A	(Phot. Set = GLYOXAL1)				GLY + HV = 0.8 HO2. + 0.45 HCHO + 1.55 CO
C58B	(Phot. Set = GLYOXAL2)				GLY + HV + #0.029 = 0.13 HCHO + 1.87 CO
C59	1.14E-11	(No T Dependence)			GLY + HO. = 0.6 HO2. + 1.2 CO + 0.4 "HCOCO-O2. + RCO3."
C60	(Same k as for CCHO)				GLY + NO3 = HNO3 + 0.6 HO2. + 1.2 CO + 0.4 "HCOCO-O2. + RCO3."
C68A	(Phot. Set = MEGLYOX1)				MGLY + HV = HO2. + CO + CCO-O2. + RCO3.
C68B	(Phot. Set = MEGLYOX2)				MGLY + HV + 0.107 = HO2. + CO + CCO-O2. + RCO3.
C69	1.72E-11	(No T Dependence)			MGLY + HO. = CO + CCO-O2. + RCO3.
C70	(Same k as for CCHO)				MGLY + NO3 = HNO3 + CO + CCO-O2. + RCO3.
G7	1.14E-11	(No T Dependence)			HO. + AFG1 = HCOCO-O2. + RCO3.
G8	(Phot. Set = ACROLEIN)				AFG1 + HV + #0.029 = HO2. + HCOCO-O2. + RCO3.
U2OH	1.72E-11	(No T Dependence)			HO. + AFG2 = C2CO-O2. + RCO3.
U2HV	(Phot. Set = ACROLEIN)				AFG2 + HV = HO2. + CO + CCO-O2. + RCO3.
G46	2.63E-11	(No T Dependence)			HO. + PHEN = 0.15 RO2-NP. + 0.85 RO2-R. + 0.2 GLY + 4.7 -C + RO2.
G51	3.60E-12	(No T Dependence)			NO3 + PHEN = HNO3 + BZ-O.
G52	4.20E-11	(No T Dependence)			HO. + CRES = 0.15 RO2-NP. + 0.85 RO2-R. + 0.2 MGLY + 5.5 -C + RO2.
G57	2.10E-11	(No T Dependence)			NO3 + CRES = HNO3 + BZ-O. + -C
G30	1.29E-11	(No T Dependence)			BALD + HO. = BZ-CO-O2. + RCO3.
G31	(Phot. Set = BZCHO)				BALD + HV + #0.05 = 7 -C
G32	2.61E-15	1.40E-12	3.75	0.00	BALD + NO3 = HNO3 + BZ-CO-O2.
G58	3.60E-12	(No T Dependence)			NPHE + NO3 = HNO3 + BZ(NO2)-O.
G59	(Same k as for BZ-O.)				BZ(NO2)-O. + NO2 = 2 -N + 6 -C
G60	(Same k as for RO2.)				BZ(NO2)-O. + HO2. = NPHE
G61	(Same k as for BZ-O.)				BZ(NO2)-O. = NPHE
C13	(Same k as for RCO3.)				CCO-O2. + NO = CO2 + NO2 + HCHO + RO2-R. + RO2.
C14	(Same k as for RCO3.)				CCO-O2. + NO2 = PAN
C15	(Same k as for RCO3.)				CCO-O2. + HO2. = -OOH + CO2 + HCHO
C16	(Same k as for RCO3.)				CCO-O2. + RO2. = RO2. + 0.5 HO2. + CO2 + HCHO
C17	(Same k as for RCO3.)				CCO-O2. + RCO3. = RCO3. + HO2. + CO2 + HCHO
C18	6.50E-04	(Falloff Kinetics)			PAN = CCO-O2. + NO2 + RCO3.
	k0 =	4.90E-03	23.97	0.00	
	kINF =	4.00E+16	27.08	0.00	
		F= 0.30	n= 1.00		
C28	(Same k as for RCO3.)				C2CO-O2. + NO = CCHO + RO2-R. + CO2 + NO2 + RO2.
C29	8.40E-12	(No T Dependence)			C2CO-O2. + NO2 = PPN
C30	(Same k as for RCO3.)				C2CO-O2. + HO2. = -OOH + CCHO + CO2
C31	(Same k as for RCO3.)				C2CO-O2. + RO2. = RO2. + 0.5 HO2. + CCHO + CO2
C32	(Same k as for RCO3.)				C2CO-O2. + RCO3. = RCO3. + HO2. + CCHO + CO2
C33	6.78E-04	1.60E+17	27.97	0.00	PPN = C2CO-O2. + NO2 + RCO3.
C62	(Same k as for RCO3.)				HCOCO-O2. + NO = NO2 + CO2 + CO + HO2.
C63	(Same k as for RCO3.)				HCOCO-O2. + NO2 = GPAN
C65	(Same k as for RCO3.)				HCOCO-O2. + HO2. = -OOH + CO2 + CO
C66	(Same k as for RCO3.)				HCOCO-O2. + RO2. = RO2. + 0.5 HO2. + CO2 + CO
C67	(Same k as for RCO3.)				HCOCO-O2. + RCO3. = RCO3. + HO2. + CO2 + CO
C64	(Same k as for PAN)				GPAN = HCOCO-O2. + NO2 + RCO3.
G33	(Same k as for RCO3.)				BZ-CO-O2. + NO = BZ-O. + CO2 + NO2 + R2O2. + RO2.
G43	3.53E-11	1.30E-11	-0.60	0.00	BZ-O. + NO2 = NPHE
G44	(Same k as for RO2.)				BZ-O. + HO2. = PHEN
G45	1.00E-03	(No T Dependence)			BZ-O. = PHEN
G34	8.40E-12	(No T Dependence)			BZ-CO-O2. + NO2 = PBZN
G36	(Same k as for RCO3.)				BZ-CO-O2. + HO2. = -OOH + CO2 + PHEN
G37	(Same k as for RCO3.)				BZ-CO-O2. + RO2. = RO2. + 0.5 HO2. + CO2 + PHEN
G38	(Same k as for RCO3.)				BZ-CO-O2. + RCO3. = RCO3. + HO2. + CO2 + PHEN
G35	2.17E-04	1.60E+15	25.90	0.00	PBZN = BZ-CO-O2. + NO2 + RCO3.
IPOH	3.36E-11	(No T Dependence)			ISOPROD + HO. = 0.293 CO + 0.252 CCHO + 0.126 HCHO + 0.041 GLY + 0.021 RCHO + 0.168 MGLY + 0.314 MEK + 0.503 RO2-R. + 0.21 CCO-O2. + 0.288 C2CO-O2. + 0.21 R2O2. + 0.713 RO2. + 0.498 RCO3. + -0.112 -C

Table A-2 (continued)

Rxn. Label	Kinetic Parameters [a] k(300)	A	Ea	B	Reactions [b]
IPO3	7.11E-18	(No T Dependence)			ISOPROD + O3 = 0.02 CCHO + 0.04 HCHO + 0.01 GLY + 0.84 MGLY + 0.09 MEK + 0.66 (HCHO2) + 0.09 (HCOCHO2) + 0.18 (HOCCHO2) + 0.06 (C2(O2)CHO) + 0.01 (C2(O2)COH) + -0.39 -C
IPHV	(Phot. Set = ACROLEIN)				ISOPROD + HV + 0.0036 = 0.333 CO + 0.067 CCHO + 0.9 HCHO + 0.033 MEK + 0.333 HO2. + 0.7 RO2-R. + 0.267 CCO-O2. + 0.7 C2CO-O2. + 0.7 RO2. + 0.967 RCO3. + -0.133 -C
IPN3	1.00E-15	(No T Dependence)			ISOPROD + NO3 = 0.643 CO + 0.282 HCHO + 0.85 RNO3 + 0.357 RCHO + 0.925 HO2. + 0.075 C2CO-O2. + 0.075 R2O2. + 0.925 RO2. + 0.075 RCO3. + 0.075 HNO3 + -2.471 -C
Hydrocarbon Species Represented Explicitly					
	2.56E-12	1.36E-12	-0.38	2.00	N-C4 + HO. = 0.076 RO2-N. + 0.924 RO2-R. + 0.397 R2O2. + 0.001 HCHO + 0.571 CCHO + 0.14 RCHO + 0.533 MEK + -0.076 -C + 1.397 RO2.
	5.63E-12	1.35E-11	0.52	0.00	N-C6 + HO. = 0.185 RO2-N. + 0.815 RO2-R. + 0.738 R2O2. + 0.02 CCHO + 0.105 RCHO + 1.134 MEK + 0.186 -C + 1.738 RO2.
	8.76E-12	3.15E-11	0.76	0.00	N-C8 + HO. = 0.333 RO2-N. + 0.667 RO2-R. + 0.706 R2O2. + 0.002 RCHO + 1.333 MEK + 0.998 -C + 1.706 RO2.
	8.43E-12	1.96E-12	-0.87	0.00	ETHENE + HO. = RO2-R. + RO2. + 1.56 HCHO + 0.22 CCHO
	1.68E-18	9.14E-15	5.13	0.00	ETHENE + O3 = HCHO + (HCHO2)
	2.18E-16	4.39E-13	4.53	2.00	ETHENE + NO3 = R2O2. + RO2. + 2 HCHO + NO2
	7.42E-13	1.04E-11	1.57	0.00	ETHENE + O = RO2-R. + HO2. + RO2. + HCHO + CO
	2.60E-11	4.85E-12	-1.00	0.00	PROPENE + HO. = RO2-R. + RO2. + HCHO + CCHO
	1.05E-17	5.51E-15	3.73	0.00	PROPENE + O3 = 0.6 HCHO + 0.4 CCHO + 0.4 (HCHO2) + 0.6 (CCHO2)
	9.74E-15	4.59E-13	2.30	0.00	PROPENE + NO3 = R2O2. + RO2. + HCHO + CCHO + NO2
	4.01E-12	1.18E-11	0.64	0.00	PROPENE + O = 0.4 HO2. + 0.5 RCHO + 0.5 MEK + -0.5 -C
	6.30E-11	1.01E-11	-1.09	0.00	T-2-BUTE + HO. = RO2-R. + RO2. + 2 CCHO
	1.95E-16	6.64E-15	2.10	0.00	T-2-BUTE + O3 = CCHO + (CCHO2)
	3.92E-13	1.10E-13	-0.76	2.00	T-2-BUTE + NO3 = R2O2. + RO2. + 2 CCHO + NO2
	2.34E-11	2.26E-11	-0.02	0.00	T-2-BUTE + O = 0.4 HO2. + 0.5 RCHO + 0.5 MEK + 0.5 -C
	9.88E-11	2.54E-11	-0.81	0.00	ISOP + HO. = 0.088 RO2-N. + 0.912 RO2-R. + 0.629 HCHO + 0.912 ISOPROD + 0.079 R2O2. + 1.079 RO2. + 0.283 -C
	1.34E-17	7.86E-15	3.80	0.00	ISOP + O3 = 0.4 HCHO + 0.6 ISOPROD + 0.55 (HCHO2) + 0.2 (C:CC(C)O2) + 0.2 (C:C(C)CHO2) + 0.05 -C
	3.60E-11	(No T Dependence)			ISOP + O = 0.75 "ISOPROD + -C "+ 0.25 "C2CO-O2. + RCO3. + 2 HCHO + RO2-R. + RO2."
	6.81E-13	3.03E-12	0.89	0.00	ISOP + NO3 = 0.8 "RCHO + RNO3 + RO2-R." + 0.2 "ISOPROD + R2O2. + NO2" + RO2. + -2.2 -C
	1.50E-19	(No T Dependence)			ISOP + NO2 = 0.8 "RCHO + RNO3 + RO2-R." + 0.2 "ISOPROD + R2O2. + NO" + RO2. + -2.2 -C
	5.31E-11	1.21E-11	-0.88	0.00	APIN + HO. = RO2-R. + RCHO + RO2. + 7 -C
	1.00E-16	9.90E-16	1.37	0.00	APIN + O3 = 0.05 HCHO + 0.2 CCHO + 0.5 RCHO + 0.61 MEK + 0.075 CO + 0.05 CCO-O2. + 0.05 C2CO-O2. + 0.1 RCO3. + 0.105 HO2. + 0.16 HO. + 0.135 RO2-R. + 0.15 R2O2. + 0.285 RO2. + 5.285 -C
	6.10E-12	1.19E-12	-0.97	0.00	APIN + NO3 = NO2 + R2O2. + RCHO + RO2. + 7 -C
	3.00E-11	(No T Dependence)			APIN + O = 0.4 HO2. + 0.5 MEK + 0.5 RCHO + 6.5 -C
	6.57E-11	(No T Dependence)			UNKN + HO. = RO2-R. + RO2. + 0.5 HCHO + RCHO + 6.5 -C
	5.85E-17	(No T Dependence)			UNKN + O3 = 0.135 RO2-R. + 0.135 HO2. + 0.075 R2O2. + 0.21 RO2. + 0.025 CCO-O2. + 0.025 C2CO-O2. + 0.05 RCO3. + 0.275 HCHO + 0.175 CCHO + 0.5 RCHO + 0.41 MEK + 0.185 CO + 5.925 -C + 0.11 HO.
	4.30E-12	(No T Dependence)			UNKN + NO3 = R2O2. + RO2. + 0.5 HCHO + RCHO + 6.5 -C + NO2
	2.90E-11	(No T Dependence)			UNKN + O = 0.4 HO2. + 0.5 RCHO + 0.5 MEK + 6.5 -C
	5.91E-12	1.81E-12	-0.70	0.00	TOLUENE + HO. = 0.085 BALD + 0.26 CRES + 0.118 GLY + 0.9638 MGLY + 0.259 AFG2 + 0.74 RO2-R. + 0.26 HO2. + 2.486 -C + 0.74 RO2.
	2.36E-11	(No T Dependence)			M-XYLENE + HO. = 0.04 BALD + 0.18 CRES + 0.108 GLY + 1.599 MGLY + 0.4612 AFG2 + 0.82 RO2-R. + 0.18 HO2. + 2.884 -C + 0.82 RO2.

Table A-2 (continued)

Rxn. Label	Kinetic Parameters [a] k(300)	A	Ea	B	Reactions [b]
Lumped Species used in EKMA Simulations [c]					
	3.46E-12	2.58E-12	-0.17	1.00	ALK1 + HO. = 0.828 RO2-R. + 0.073 RO2-N. + 0.005 RO2-XN. + 0.011 HO2. + 0.574 R2O2. + 1.48 RO2. + 0.021 HO. + 0.022 HCHO + 0.339 CCHO + 0.176 RCHO + 0.26 ACET + 0.447 MEK + 0.024 CO + 0.026 GLY2 + 0.062 C2(C)-O. + 0.142 -C
	9.14E-12	5.12E-12	-0.35	1.00	ALK2 + HO. = 0.749 RO2-R. + 0.249 RO2-N. + 0.002 RO2-XN. + 0.891 R2O2. + 1.891 RO2. + 0.029 HCHO + 0.048 CCHO + 0.288 RCHO + 0.028 ACET + 1.105 MEK + 0.043 CO + 0.018 CO2 + 1.268 -C
	5.87E-12	(No T Dependence)			ARO1 + HO. = 0.742 RO2-R. + 0.258 HO2. + 0.742 RO2. + 0.015 PHEN + 0.244 CRES + 0.08 BALD + 0.124 GLY + 0.773 MGLY + 0.091 AFG1 + 0.229 AFG2 + 1.665 -C
	3.22E-11	1.20E-11	-0.59	1.00	ARO2 + HO. = 0.82 RO2-R. + 0.18 HO2. + 0.82 RO2. + 0.18 CRES + 0.036 BALD + 0.068 GLY + 1.159 MGLY + 0.49 AFG2 + 2.297 -C
	3.17E-11	2.22E-12	-1.59	1.00	OLE1 + HO. = 0.858 RO2-R. + 0.142 RO2-N. + RO2. + 0.858 HCHO + 0.252 CCHO + 0.606 RCHO + 1.267 -C
	1.08E-17	1.42E-15	2.91	1.00	OLE1 + O3 = 0.6 HCHO + 0.635 RCHO + 0.981 -C + 0.4 (HCHO2) + 0.529 (CCHO2) + 0.071 (RCHO2)
	1.16E-14	1.99E-13	1.69	1.00	OLE1 + NO3 = R2O2. + RO2. + HCHO + 0.294 CCHO + 0.706 RCHO + 1.451 -C + NO2
	4.11E-12	4.51E-12	0.06	1.00	OLE1 + O = 0.4 HO2. + 0.5 RCHO + 0.5 MEK + 1.657 -C
	6.23E-11	4.54E-12	-1.56	1.00	OLE2 + HO. = 0.861 RO2-R. + 0.139 RO2-N. + RO2. + 0.24 HCHO + 0.661 CCHO + 0.506 RCHO + 0.113 ACET + 0.086 MEK + 0.057 BALD + 0.848 -C
	1.70E-16	1.77E-15	1.40	1.00	OLE2 + O3 = 0.203 HCHO + 0.358 CCHO + 0.309 RCHO + 0.061 MEK + 0.027 BALD + 0.976 -C + 0.076 (HCHO2) + 0.409 (CCHO2) + 0.279 (RCHO2) + 0.158 (C(C)CO2 + 0.039 (C(R)CO2 + 0.04 (BZCHO2)
	1.07E-12	3.19E-13	-0.72	1.00	OLE2 + NO3 = R2O2. + RO2. + 0.278 HCHO + 0.767 CCHO + 0.588 RCHO + 0.131 ACET + 0.1 MEK + 0.066 BALD + 0.871 -C + NO2
	2.52E-11	8.66E-12	-0.64	1.00	OLE2 + O = 0.4 HO2. + 0.5 RCHO + 0.5 MEK + 2.205 -C
Propylene Glycol (kOH as used in the Atmospheric Reactivity Simulations) [e]					
	2.23E-11 (T dependence ignored)				PR-GLYCL + HO. = HO2. + 0.314 RCHO + 0.686 "MEK - -C"
Reactions used to Represent Chamber-Dependent Processes [f]					
O3W	(varied)	(No T Dependence)			O3 =
N25I	(varied)	(No T Dependence)			N2O5 = 2 NOX-WALL
N25S	(varied)	(No T Dependence)			N2O5 + H2O = 2 NOX-WALL
NO2W	(varied)	(No T Dependence)			NO2 = (yHONO) HONO + (1-yHONO) NOX-WALL
XSHC	(varied)	(No T Dependence)			HO. = HO2.
RSI	(Phot. Set = NO2)				HV + #RS/K1 = HO.
ONO2	(Phot. Set = NO2)				HV + #E-NO2/K1 = NO2 + #-1 NOX-WALL

[a] Except as noted, expression for rate constant is k = A $e^{Ea/RT}$ $(T/300)^{B}$. Rate constants and A factor are in cm, molecule, sec. units. Units of Ea is kcal $mole^{-1}$. "Phot Set" means this is a photolysis reaction, with the absorption coefficients and quantum yields given in Table A-3. In addition, if "#(number)" or "#(parameter)" is given as a reactant, then the value of that number or parameter is multiplied by the result in the "rate constant expression" columns to obtain the rate constant used. Furthermore, "#RCONnn" as a reactant means that the rate constant for the reaction is obtained by multiplying the rate constant given by that for reaction "nn". Thus, the rate constant given is actually an equilibrium constant.

[b] Format of reaction listing same as used in documentation of the detailed mechanism (Carter 1990).

[c] Rate constants and product yield parameters based on the mixture of species in the base ROG mixture which are being represented.

[d] Not used in atmospheric reactivity simulations because of poor performance in simulating the chamber data.

[e] Rate constant used in the atmospheric reactivity simulations is from Aschmann and Atkinson (1997). Chamber simulations were also carried out using kOH = 1.2 x 10^{-11} cm^3 $molec^{-1}$ s^{-1} (Wiedelmann and Zetzch, 1992) and kOH = 2.8 x 10^{-11} cm^3 $molec^{-1}$ s^{-1}, as derived from the PG vs m-xylene consumption rates in the chamber experiments.

[f] See Table A-4 for the values of the parameters used for the specific chambers modeled in this study.

Table A-3. Absorption cross sections and quantum yields for photolysis reactions.

WL (nm)	Abs (cm^2)	QY	WL (nm)	Abs (cm^2)	QY	WL (nm)	Abs (cm^2)	QY	WL (nm)	Abs (cm^2)	QY	WL (nm)	Abs (cm^2)	QY
Photolysis File = NO2														
250.0	2.83E-20	1.000	255.0	1.45E-20	1.000	260.0	1.90E-20	1.000	265.0	2.05E-20	1.000	270.0	3.13E-20	1.000
275.0	4.02E-20	1.000	280.0	5.54E-20	1.000	285.0	6.99E-20	1.000	290.0	8.18E-20	0.999	295.0	9.67E-20	0.998
300.0	1.17E-19	0.997	305.0	1.66E-19	0.996	310.0	1.76E-19	0.995	315.0	2.25E-19	0.994	320.0	2.54E-19	0.993
325.0	2.79E-19	0.992	330.0	2.99E-19	0.991	335.0	3.45E-19	0.990	340.0	3.88E-19	0.989	345.0	4.07E-19	0.988
350.0	4.10E-19	0.987	355.0	5.13E-19	0.986	360.0	4.51E-19	0.984	365.0	5.78E-19	0.983	370.0	5.42E-19	0.981
375.0	5.35E-19	0.979	380.0	5.99E-19	0.975	381.0	5.98E-19	0.974	382.0	5.97E-19	0.973	383.0	5.96E-19	0.972
384.0	5.95E-19	0.971	385.0	5.94E-19	0.969	386.0	5.95E-19	0.967	387.0	5.96E-19	0.966	388.0	5.98E-19	0.964
389.0	5.99E-19	0.962	390.0	6.00E-19	0.960	391.0	5.98E-19	0.959	392.0	5.96E-19	0.957	393.0	5.93E-19	0.953
394.0	5.91E-19	0.950	395.0	5.89E-19	0.942	396.0	6.06E-19	0.922	397.0	6.24E-19	0.870	398.0	6.41E-19	0.820
399.0	6.59E-19	0.760	400.0	6.76E-19	0.695	401.0	6.67E-19	0.635	402.0	6.58E-19	0.560	403.0	6.50E-19	0.485
404.0	6.41E-19	0.425	405.0	6.32E-19	0.350	406.0	6.21E-19	0.290	407.0	6.10E-19	0.225	408.0	5.99E-19	0.185
409.0	5.88E-19	0.153	410.0	5.77E-19	0.130	411.0	5.88E-19	0.110	412.0	5.98E-19	0.094	413.0	6.09E-19	0.083
414.0	6.19E-19	0.070	415.0	6.30E-19	0.059	416.0	6.29E-19	0.048	417.0	6.27E-19	0.039	418.0	6.26E-19	0.030
419.0	6.24E-19	0.023	420.0	6.23E-19	0.018	421.0	6.18E-19	0.012	422.0	6.14E-19	0.008	423.0	6.09E-19	0.004
424.0	6.05E-19	0.000	425.0	6.00E-19	0.000									
Photolysis File = NO3NO														
585.0	2.77E-18	0.000	590.0	5.14E-18	0.250	595.0	4.08E-18	0.400	600.0	2.83E-18	0.250	605.0	3.45E-18	0.200
610.0	1.48E-18	0.200	615.0	1.96E-18	0.100	620.0	3.58E-18	0.100	625.0	9.25E-18	0.050	630.0	5.66E-18	0.050
635.0	1.45E-18	0.030	640.0	1.11E-18	0.000									
Photolysis File = NO3NO2														
400.0	0.00E+00	1.000	405.0	3.00E-20	1.000	410.0	4.00E-20	1.000	415.0	5.00E-20	1.000	420.0	8.00E-20	1.000
425.0	1.00E-19	1.000	430.0	1.30E-19	1.000	435.0	1.80E-19	1.000	440.0	1.90E-19	1.000	445.0	2.20E-19	1.000
450.0	2.80E-19	1.000	455.0	3.30E-19	1.000	460.0	3.70E-19	1.000	465.0	4.30E-19	1.000	470.0	5.10E-19	1.000
475.0	6.00E-19	1.000	480.0	6.40E-19	1.000	485.0	6.90E-19	1.000	490.0	8.80E-19	1.000	495.0	9.50E-19	1.000
500.0	1.01E-18	1.000	505.0	1.10E-18	1.000	510.0	1.32E-18	1.000	515.0	1.40E-18	1.000	520.0	1.45E-18	1.000
525.0	1.48E-18	1.000	530.0	1.94E-18	1.000	535.0	2.04E-18	1.000	540.0	1.81E-18	1.000	545.0	1.81E-18	1.000
550.0	2.36E-18	1.000	555.0	2.68E-18	1.000	560.0	3.07E-18	1.000	565.0	2.53E-18	1.000	570.0	2.54E-18	1.000
575.0	2.74E-18	1.000	580.0	3.05E-18	1.000	585.0	2.77E-18	1.000	590.0	5.14E-18	0.750	595.0	4.08E-18	0.600
600.0	2.83E-18	0.550	605.0	3.45E-18	0.400	610.0	1.45E-18	0.300	615.0	1.96E-18	0.250	620.0	3.58E-18	0.200
625.0	9.25E-18	0.150	630.0	5.66E-18	0.050	635.0	1.45E-18	0.000						
Photolysis File = O3O3P														
280.0	3.97E-18	0.100	281.0	3.60E-18	0.100	282.0	3.24E-18	0.100	283.0	3.01E-18	0.100	284.0	2.73E-18	0.100
285.0	2.44E-18	0.100	286.0	2.21E-18	0.100	287.0	2.01E-18	0.100	288.0	1.76E-18	0.100	289.0	1.58E-18	0.100
290.0	1.41E-18	0.100	291.0	1.26E-18	0.100	292.0	1.10E-18	0.100	293.0	9.89E-19	0.100	294.0	8.59E-19	0.100
295.0	7.70E-19	0.100	296.0	6.67E-19	0.100	297.0	5.84E-19	0.100	298.0	5.07E-19	0.100	299.0	4.52E-19	0.100
300.0	3.92E-19	0.100	301.0	3.42E-19	0.100	302.0	3.06E-19	0.100	303.0	2.60E-19	0.100	304.0	2.37E-19	0.100
305.0	2.01E-19	0.112	306.0	1.79E-19	0.149	307.0	1.56E-19	0.197	308.0	1.38E-19	0.259	309.0	1.25E-19	0.339
310.0	1.02E-19	0.437	311.0	9.17E-20	0.546	312.0	7.88E-20	0.652	313.0	6.77E-20	0.743	314.0	6.35E-20	0.816
315.0	5.10E-20	0.872	316.0	4.61E-20	0.916	317.0	4.17E-20	0.949	318.0	3.72E-20	0.976	319.0	2.69E-20	0.997
320.0	3.23E-20	1.000	330.0	6.70E-21	1.000	340.0	1.70E-21	1.000	350.0	4.00E-22	1.000	355.0	0.00E+00	1.000
400.0	0.00E+00	1.000	450.0	1.60E-22	1.000	500.0	1.34E-21	1.000	550.0	3.32E-21	1.000	600.0	5.06E-21	1.000
650.0	2.45E-21	1.000	700.0	8.70E-22	1.000	750.0	3.20E-22	1.000	800.0	1.60E-22	1.000	900.0	0.00E+00	1.000
Photolysis File = O3O1D														
280.0	3.97E-18	0.900	281.0	3.60E-18	0.900	282.0	3.24E-18	0.900	283.0	3.01E-18	0.900	284.0	2.73E-18	0.900
285.0	2.44E-18	0.900	286.0	2.21E-18	0.900	287.0	2.01E-18	0.900	288.0	1.76E-18	0.900	289.0	1.58E-18	0.900
290.0	1.41E-18	0.900	291.0	1.26E-18	0.900	292.0	1.10E-18	0.900	293.0	9.89E-19	0.900	294.0	8.59E-19	0.900
295.0	7.70E-19	0.900	296.0	6.67E-19	0.900	297.0	5.84E-19	0.900	298.0	5.07E-19	0.900	299.0	4.52E-19	0.900
300.0	3.92E-19	0.900	301.0	3.42E-19	0.900	302.0	3.06E-19	0.900	303.0	2.60E-19	0.900	304.0	2.37E-19	0.900
305.0	2.01E-19	0.888	306.0	1.79E-19	0.851	307.0	1.56E-19	0.803	308.0	1.38E-19	0.741	309.0	1.25E-19	0.661
310.0	1.02E-19	0.563	311.0	9.17E-20	0.454	312.0	7.88E-20	0.348	313.0	6.77E-20	0.257	314.0	6.35E-20	0.184
315.0	5.10E-20	0.128	316.0	4.61E-20	0.084	317.0	4.17E-20	0.051	318.0	3.72E-20	0.024	319.0	2.69E-20	0.003
320.0	3.23E-20	0.000												
Photolysis File = HONO														
311.0	0.00E+00	1.000	312.0	2.00E-21	1.000	313.0	4.20E-21	1.000	314.0	4.60E-21	1.000	315.0	4.20E-21	1.000
316.0	3.00E-21	1.000	317.0	4.60E-21	1.000	318.0	3.60E-20	1.000	319.0	6.10E-20	1.000	320.0	2.10E-20	1.000
321.0	4.27E-20	1.000	322.0	4.01E-20	1.000	323.0	3.93E-20	1.000	324.0	4.01E-20	1.000	325.0	4.04E-20	1.000
326.0	3.13E-20	1.000	327.0	4.12E-20	1.000	328.0	7.55E-20	1.000	329.0	6.64E-20	1.000	330.0	7.29E-20	1.000
331.0	8.70E-20	1.000	332.0	1.38E-19	1.000	333.0	5.91E-20	1.000	334.0	5.91E-20	1.000	335.0	6.45E-20	1.000
336.0	5.91E-20	1.000	337.0	4.58E-20	1.000	338.0	1.91E-19	1.000	339.0	1.63E-19	1.000	340.0	1.05E-19	1.000
341.0	8.70E-20	1.000	342.0	3.35E-19	1.000	343.0	2.01E-19	1.000	344.0	1.02E-19	1.000	345.0	8.54E-20	1.000
346.0	8.32E-20	1.000	347.0	8.20E-20	1.000	348.0	7.49E-20	1.000	349.0	7.13E-20	1.000	350.0	6.83E-20	1.000
351.0	1.74E-19	1.000	352.0	1.14E-19	1.000	353.0	3.71E-19	1.000	354.0	4.96E-19	1.000	355.0	2.46E-19	1.000
356.0	1.19E-19	1.000	357.0	9.35E-20	1.000	358.0	7.78E-20	1.000	359.0	7.29E-20	1.000	360.0	6.83E-20	1.000
361.0	6.90E-20	1.000	362.0	7.32E-20	1.000	363.0	9.00E-20	1.000	364.0	1.21E-19	1.000	365.0	1.33E-19	1.000
366.0	2.13E-19	1.000	367.0	3.52E-19	1.000	368.0	4.50E-19	1.000	369.0	2.93E-19	1.000	370.0	1.19E-19	1.000
371.0	9.46E-20	1.000	372.0	8.85E-20	1.000	373.0	7.44E-20	1.000	374.0	4.77E-20	1.000	375.0	2.70E-20	1.000
376.0	1.90E-20	1.000	377.0	1.50E-20	1.000	378.0	1.90E-20	1.000	379.0	5.80E-20	1.000	380.0	7.78E-20	1.000
381.0	1.14E-19	1.000	382.0	1.40E-19	1.000	383.0	1.72E-19	1.000	384.0	1.99E-19	1.000	385.0	1.90E-19	1.000
386.0	1.19E-19	1.000	387.0	5.65E-20	1.000	388.0	3.20E-20	1.000	389.0	1.90E-20	1.000	390.0	1.20E-20	1.000
391.0	5.00E-21	1.000	392.0	0.00E+00	1.000									
Photolysis File = H2O2														
250.0	8.30E-20	1.000	255.0	6.70E-20	1.000	260.0	5.20E-20	1.000	265.0	4.20E-20	1.000	270.0	3.20E-20	1.000
275.0	2.50E-20	1.000	280.0	2.00E-20	1.000	285.0	1.50E-20	1.000	290.0	1.13E-20	1.000	295.0	8.70E-21	1.000
300.0	6.60E-21	1.000	305.0	4.90E-21	1.000	310.0	3.70E-21	1.000	315.0	2.80E-21	1.000	320.0	2.00E-21	1.000
325.0	1.50E-21	1.000	330.0	1.20E-21	1.000	335.0	9.00E-22	1.000	340.0	7.00E-22	1.000	345.0	5.00E-22	1.000
350.0	3.00E-22	1.000	355.0	0.00E+00	1.000									

Table A-3. (continued)

WL (nm)	Abs (cm^2)	QY	WL (nm)	Abs (cm^2)	QY	WL (nm)	Abs (cm^2)	QY	WL (nm)	Abs (cm^2)	QY	WL (nm)	Abs (cm^2)	QY
Photolysis File = CO2H														
210.0	3.75E-19	1.000	220.0	2.20E-19	1.000	230.0	1.38E-19	1.000	240.0	8.80E-20	1.000	250.0	5.80E-20	1.000
260.0	3.80E-20	1.000	270.0	2.50E-20	1.000	280.0	1.50E-20	1.000	290.0	9.00E-21	1.000	300.0	5.80E-21	1.000
310.0	3.40E-21	1.000	320.0	1.90E-21	1.000	330.0	1.10E-21	1.000	340.0	6.00E-22	1.000	350.0	4.00E-22	1.000
360.0	0.00E+00	1.000												
Photolysis File = HCHONEWR														
280.0	2.49E-20	0.590	280.5	1.42E-20	0.596	281.0	1.51E-20	0.602	281.5	1.32E-20	0.608	282.0	9.73E-21	0.614
282.5	6.76E-21	0.620	283.0	5.82E-21	0.626	283.5	9.10E-21	0.632	284.0	3.71E-20	0.638	284.5	4.81E-20	0.644
285.0	3.95E-20	0.650	285.5	2.87E-20	0.656	286.0	2.24E-20	0.662	286.5	1.74E-20	0.668	287.0	1.13E-20	0.674
287.5	1.10E-20	0.680	288.0	2.62E-20	0.686	288.5	4.00E-20	0.692	289.0	3.55E-20	0.698	289.5	2.12E-20	0.704
290.0	1.07E-20	0.710	290.5	1.35E-20	0.713	291.0	1.99E-20	0.717	291.5	1.56E-20	0.721	292.0	8.65E-21	0.724
292.5	5.90E-21	0.727	293.0	1.11E-20	0.731	293.5	6.26E-20	0.735	294.0	7.40E-20	0.738	294.5	5.36E-20	0.741
295.0	4.17E-20	0.745	295.5	3.51E-20	0.749	296.0	2.70E-20	0.752	296.5	1.75E-20	0.755	297.0	1.16E-20	0.759
297.5	1.51E-20	0.763	298.0	3.69E-20	0.766	298.5	4.40E-20	0.769	299.0	3.44E-20	0.773	299.5	2.02E-20	0.776
300.0	1.06E-20	0.780	300.4	7.01E-21	0.780	300.6	8.63E-21	0.779	300.8	1.47E-20	0.779	301.0	2.01E-20	0.779
301.2	2.17E-20	0.779	301.4	1.96E-20	0.779	301.6	1.54E-20	0.778	301.8	1.26E-20	0.778	302.0	1.03E-20	0.778
302.2	8.53E-21	0.778	302.4	7.13E-21	0.778	302.6	6.61E-21	0.777	302.8	1.44E-20	0.777	303.0	3.18E-20	0.777
303.2	3.81E-20	0.777	303.4	5.57E-20	0.777	303.6	6.91E-20	0.776	303.8	6.58E-20	0.776	304.0	6.96E-20	0.776
304.2	5.79E-20	0.776	304.4	5.24E-20	0.776	304.6	4.30E-20	0.775	304.8	3.28E-20	0.775	305.0	3.60E-20	0.775
305.2	5.12E-20	0.775	305.4	4.77E-20	0.775	305.6	4.43E-20	0.774	305.8	4.60E-20	0.774	306.0	4.01E-20	0.774
306.2	3.28E-20	0.774	306.4	2.66E-20	0.774	306.6	2.42E-20	0.773	306.8	1.95E-20	0.773	307.0	1.58E-20	0.773
307.2	1.37E-20	0.773	307.4	1.19E-20	0.773	307.6	1.01E-20	0.772	307.8	9.01E-21	0.772	308.0	8.84E-21	0.772
308.2	2.08E-20	0.772	308.4	2.39E-20	0.772	308.6	3.08E-20	0.771	308.8	3.39E-20	0.771	309.0	3.18E-20	0.771
309.2	3.06E-20	0.771	309.4	2.84E-20	0.771	309.6	2.46E-20	0.770	309.8	1.95E-20	0.770	310.0	1.57E-20	0.770
310.2	1.26E-20	0.767	310.4	9.26E-21	0.764	310.6	7.71E-21	0.761	310.8	6.05E-21	0.758	311.0	5.13E-21	0.755
311.2	4.82E-21	0.752	311.4	4.54E-21	0.749	311.6	6.81E-21	0.746	311.8	1.04E-20	0.743	312.0	1.43E-20	0.740
312.2	1.47E-20	0.737	312.4	1.35E-20	0.734	312.6	1.13E-20	0.731	312.8	9.86E-21	0.728	313.0	7.82E-21	0.725
313.2	6.48E-21	0.722	313.4	1.07E-20	0.719	313.6	2.39E-20	0.716	313.8	3.80E-20	0.713	314.0	5.76E-20	0.710
314.2	6.14E-20	0.707	314.4	7.45E-20	0.704	314.6	5.78E-20	0.701	314.8	5.59E-20	0.698	315.0	4.91E-20	0.695
315.2	4.37E-20	0.692	315.4	3.92E-20	0.689	315.6	2.89E-20	0.686	315.8	2.82E-20	0.683	316.0	2.10E-20	0.680
316.2	1.66E-20	0.677	316.4	2.05E-20	0.674	316.6	4.38E-20	0.671	316.8	5.86E-20	0.668	317.0	6.28E-20	0.665
317.2	5.07E-20	0.662	317.4	4.33E-20	0.659	317.6	4.17E-20	0.656	317.8	3.11E-20	0.653	318.0	2.64E-20	0.650
318.2	2.24E-20	0.647	318.4	1.70E-20	0.644	318.6	1.24E-20	0.641	318.8	1.11E-20	0.638	319.0	7.70E-21	0.635
319.2	6.36E-21	0.632	319.4	5.36E-21	0.629	319.6	4.79E-21	0.626	319.8	6.48E-21	0.623	320.0	1.48E-20	0.620
320.2	1.47E-20	0.614	320.4	1.36E-20	0.608	320.6	1.69E-20	0.601	320.8	1.32E-20	0.595	321.0	1.49E-20	0.589
321.2	1.17E-20	0.583	321.4	1.15E-20	0.577	321.6	9.64E-21	0.570	321.8	7.26E-21	0.564	322.0	5.94E-21	0.558
322.2	4.13E-21	0.552	322.4	3.36E-21	0.546	322.6	2.39E-21	0.539	322.8	2.01E-21	0.533	323.0	1.76E-21	0.527
323.2	2.82E-21	0.521	323.4	4.65E-21	0.515	323.6	7.00E-21	0.508	323.8	7.80E-21	0.502	324.0	7.87E-21	0.496
324.2	6.59E-21	0.490	324.4	5.60E-21	0.484	324.6	4.66E-21	0.477	324.8	4.21E-21	0.471	325.0	7.77E-21	0.465
325.2	2.15E-20	0.459	325.4	3.75E-20	0.453	325.6	4.10E-20	0.446	325.8	6.47E-20	0.440	326.0	7.59E-20	0.434
326.2	6.51E-20	0.428	326.4	5.53E-20	0.422	326.6	5.76E-20	0.415	326.8	4.43E-20	0.409	327.0	3.44E-20	0.403
327.2	3.22E-20	0.397	327.4	2.13E-20	0.391	327.6	1.91E-20	0.384	327.8	1.42E-20	0.378	328.0	9.15E-21	0.372
328.2	6.79E-21	0.366	328.4	4.99E-21	0.360	328.6	4.77E-21	0.353	328.8	1.75E-20	0.347	329.0	3.27E-20	0.341
329.2	3.99E-20	0.335	329.4	5.13E-20	0.329	329.6	4.00E-20	0.322	329.8	3.61E-20	0.316	330.0	3.38E-20	0.310
330.2	3.08E-20	0.304	330.4	2.16E-20	0.298	330.6	2.09E-20	0.291	330.8	1.41E-20	0.285	331.0	9.95E-21	0.279
331.2	7.76E-21	0.273	331.4	6.16E-21	0.267	331.6	4.06E-21	0.260	331.8	3.03E-21	0.254	332.0	2.41E-21	0.248
332.2	1.74E-21	0.242	332.4	1.33E-21	0.236	332.6	2.70E-21	0.229	332.8	1.65E-21	0.223	333.0	1.17E-21	0.217
333.2	9.84E-22	0.211	333.4	8.52E-22	0.205	333.6	6.32E-22	0.198	333.8	5.21E-22	0.192	334.0	1.46E-21	0.186
334.2	1.80E-21	0.180	334.4	1.43E-21	0.174	334.6	1.03E-21	0.167	334.8	7.19E-22	0.161	335.0	4.84E-22	0.155
335.2	2.73E-22	0.149	335.4	1.34E-22	0.143	335.6	-1.62E-22	0.136	335.8	1.25E-22	0.130	336.0	4.47E-22	0.124
336.2	1.23E-21	0.118	336.4	2.02E-21	0.112	336.6	3.00E-21	0.105	336.8	2.40E-21	0.099	337.0	3.07E-21	0.093
337.2	2.29E-21	0.087	337.4	2.46E-21	0.081	337.6	2.92E-21	0.074	337.8	8.10E-21	0.068	338.0	1.82E-20	0.062
338.2	3.10E-20	0.056	338.4	3.24E-20	0.050	338.6	4.79E-20	0.043	338.8	5.25E-20	0.037	339.0	5.85E-20	0.031
339.2	4.33E-20	0.025	339.4	4.20E-20	0.019	339.6	3.99E-20	0.012	339.8	3.11E-20	0.006	340.0	2.72E-20	0.000
Photolysis File = HCHONEWM														
280.0	2.49E-20	0.350	280.5	1.42E-20	0.346	281.0	1.51E-20	0.341	281.5	1.32E-20	0.336	282.0	9.73E-21	0.332
282.5	6.76E-21	0.327	283.0	5.82E-21	0.323	283.5	9.10E-21	0.319	284.0	3.71E-20	0.314	284.5	4.81E-20	0.309
285.0	3.95E-20	0.305	285.5	2.87E-20	0.301	286.0	2.24E-20	0.296	286.5	1.74E-20	0.291	287.0	1.13E-20	0.287
287.5	1.10E-20	0.282	288.0	2.62E-20	0.278	288.5	4.00E-20	0.273	289.0	3.55E-20	0.269	289.5	2.12E-20	0.264
290.0	1.07E-20	0.260	290.5	1.35E-20	0.258	291.0	1.99E-20	0.256	291.5	1.56E-20	0.254	292.0	8.65E-21	0.252
292.5	5.90E-21	0.250	293.0	1.11E-20	0.248	293.5	6.26E-20	0.246	294.0	7.40E-20	0.244	294.5	5.36E-20	0.242
295.0	4.17E-20	0.240	295.5	3.51E-20	0.238	296.0	2.70E-20	0.236	296.5	1.75E-20	0.234	297.0	1.16E-20	0.232
297.5	1.51E-20	0.230	298.0	3.69E-20	0.228	298.5	4.40E-20	0.226	299.0	3.44E-20	0.224	299.5	2.02E-20	0.222
300.0	1.06E-20	0.220	300.4	7.01E-21	0.220	300.6	8.63E-21	0.221	300.8	1.47E-20	0.221	301.0	2.01E-20	0.221
301.2	2.17E-20	0.221	301.4	1.96E-20	0.221	301.6	1.54E-20	0.222	301.8	1.26E-20	0.222	302.0	1.03E-20	0.222
302.2	8.53E-21	0.222	302.4	7.13E-21	0.222	302.6	6.61E-21	0.223	302.8	1.44E-20	0.223	303.0	3.18E-20	0.223
303.2	3.81E-20	0.223	303.4	5.57E-20	0.223	303.6	6.91E-20	0.224	303.8	6.58E-20	0.224	304.0	6.96E-20	0.224
304.2	5.79E-20	0.224	304.4	5.24E-20	0.224	304.6	4.30E-20	0.225	304.8	3.28E-20	0.225	305.0	3.60E-20	0.225
305.2	5.12E-20	0.225	305.4	4.77E-20	0.225	305.6	4.43E-20	0.226	305.8	4.60E-20	0.226	306.0	4.01E-20	0.226
306.2	3.28E-20	0.226	306.4	2.66E-20	0.226	306.6	2.42E-20	0.227	306.8	1.95E-20	0.227	307.0	1.58E-20	0.227
307.2	1.37E-20	0.227	307.4	1.19E-20	0.227	307.6	1.01E-20	0.228	307.8	9.01E-21	0.228	308.0	8.84E-21	0.228
308.2	2.08E-20	0.228	308.4	2.39E-20	0.228	308.6	3.08E-20	0.229	308.8	3.39E-20	0.229	309.0	3.18E-20	0.229
309.2	3.06E-20	0.229	309.4	2.84E-20	0.229	309.6	2.46E-20	0.230	309.8	1.95E-20	0.230	310.0	1.57E-20	0.230
310.2	1.26E-20	0.233	310.4	9.26E-21	0.236	310.6	7.71E-21	0.239	310.8	6.05E-21	0.242	311.0	5.13E-21	0.245
311.2	4.82E-21	0.248	311.4	4.54E-21	0.251	311.6	6.81E-21	0.254	311.8	1.04E-20	0.257	312.0	1.43E-20	0.260
312.2	1.47E-20	0.263	312.4	1.35E-20	0.266	312.6	1.13E-20	0.269	312.8	9.86E-21	0.272	313.0	7.82E-21	0.275
313.2	6.48E-21	0.278	313.4	1.07E-20	0.281	313.6	2.39E-20	0.284	313.8	3.80E-20	0.287	314.0	5.76E-20	0.290
314.2	6.14E-20	0.293	314.4	7.45E-20	0.296	314.6	5.78E-20	0.299	314.8	5.59E-20	0.302	315.0	4.91E-20	0.305
315.2	4.37E-20	0.308	315.4	3.92E-20	0.311	315.6	2.89E-20	0.314	315.8	2.82E-20	0.317	316.0	2.10E-20	0.320
316.2	1.66E-20	0.323	316.4	2.05E-20	0.326	316.6	4.38E-20	0.329	316.8	5.86E-20	0.332	317.0	6.28E-20	0.335
317.2	5.07E-20	0.338	317.4	4.33E-20	0.341	317.6	4.17E-20	0.344	317.8	3.11E-20	0.347	318.0	2.64E-20	0.350
318.2	2.24E-20	0.353	318.4	1.70E-20	0.356	318.6	1.24E-20	0.359	318.8	1.11E-20	0.362	319.0	7.70E-21	0.365
319.2	6.36E-21	0.368	319.4	5.36E-21	0.371	319.6	4.79E-21	0.374	319.8	6.48E-21	0.377	320.0	1.48E-20	0.380
320.2	1.47E-20	0.386	320.4	1.36E-20	0.392	320.6	1.69E-20	0.399	320.8	1.32E-20	0.405	321.0	1.49E-20	0.411
321.2	1.17E-20	0.417	321.4	1.15E-20	0.423	321.6	9.64E-21	0.430	321.8	7.26E-21	0.436	322.0	5.94E-21	0.442

Table A-3. (continued)

WL (nm)	Abs (cm^2)	QY	WL (nm)	Abs (cm^2)	QY	WL (nm)	Abs (cm^2)	QY	WL (nm)	Abs (cm^2)	QY	WL (nm)	Abs (cm^2)	QY
322.2	4.13E-21	0.448	322.4	3.36E-21	0.454	322.6	2.39E-21	0.461	322.8	2.01E-21	0.467	323.0	1.76E-21	0.473
323.2	2.82E-21	0.479	323.4	4.65E-21	0.485	323.6	7.00E-21	0.492	323.8	7.80E-21	0.498	324.0	7.87E-21	0.504
324.2	6.59E-21	0.510	324.4	5.60E-21	0.516	324.6	4.66E-21	0.523	324.8	4.21E-21	0.529	325.0	7.77E-21	0.535
325.2	2.15E-20	0.541	325.4	3.75E-20	0.547	325.6	4.10E-20	0.554	325.8	6.47E-20	0.560	326.0	7.59E-20	0.566
326.2	6.51E-20	0.572	326.4	5.53E-20	0.578	326.6	5.76E-20	0.585	326.8	4.43E-20	0.591	327.0	3.44E-20	0.597
327.2	3.22E-20	0.603	327.4	2.13E-20	0.609	327.6	1.91E-20	0.616	327.8	1.42E-20	0.622	328.0	9.15E-21	0.628
328.2	6.79E-21	0.634	328.4	4.99E-21	0.640	328.6	4.77E-21	0.647	328.8	1.75E-20	0.653	329.0	3.27E-20	0.659
329.2	3.99E-20	0.665	329.4	5.13E-20	0.671	329.6	4.00E-20	0.678	329.8	3.61E-20	0.684	330.0	3.38E-20	0.690
330.2	3.08E-20	0.694	330.4	2.16E-20	0.699	330.6	2.09E-20	0.703	330.8	1.41E-20	0.708	331.0	9.95E-21	0.712
331.2	7.76E-21	0.717	331.4	6.16E-21	0.721	331.6	4.06E-21	0.726	331.8	3.03E-21	0.730	332.0	2.41E-21	0.735
332.2	1.74E-21	0.739	332.4	1.33E-21	0.744	332.6	2.70E-21	0.748	332.8	1.65E-21	0.753	333.0	1.17E-21	0.757
333.2	9.84E-22	0.762	333.4	8.52E-22	0.766	333.6	6.32E-22	0.771	333.8	5.21E-22	0.775	334.0	1.46E-21	0.780
334.2	1.80E-21	0.784	334.4	1.43E-21	0.789	334.6	1.03E-21	0.793	334.8	7.19E-22	0.798	335.0	4.84E-22	0.802
335.2	2.73E-22	0.798	335.4	1.34E-22	0.794	335.6	0.00E+00	0.790	335.8	1.25E-22	0.786	336.0	4.47E-22	0.782
336.2	1.23E-21	0.778	336.4	2.02E-21	0.773	336.6	3.00E-21	0.769	336.8	2.40E-21	0.764	337.0	3.07E-21	0.759
337.2	2.29E-21	0.754	337.4	2.46E-21	0.749	337.6	2.92E-21	0.745	337.8	8.10E-21	0.740	338.0	1.82E-20	0.734
338.2	3.10E-20	0.729	338.4	3.24E-20	0.724	338.6	4.79E-20	0.719	338.8	5.25E-20	0.714	339.0	5.85E-20	0.709
339.2	4.33E-20	0.703	339.4	4.20E-20	0.698	339.6	3.99E-20	0.693	339.8	3.11E-20	0.687	340.0	2.72E-20	0.682
340.2	1.99E-20	0.676	340.4	1.76E-20	0.671	340.6	1.39E-20	0.666	340.8	1.01E-20	0.660	341.0	6.57E-21	0.655
341.2	4.83E-21	0.649	341.4	3.47E-21	0.643	341.6	2.23E-21	0.638	341.8	1.55E-21	0.632	342.0	3.70E-21	0.627
342.2	4.64E-21	0.621	342.4	1.08E-20	0.616	342.6	1.14E-20	0.610	342.8	1.79E-20	0.604	343.0	2.33E-20	0.599
343.2	1.72E-20	0.593	343.4	1.55E-20	0.588	343.6	1.46E-20	0.582	343.8	1.38E-20	0.576	344.0	1.00E-20	0.571
344.2	8.26E-21	0.565	344.4	6.32E-21	0.559	344.6	4.28E-21	0.554	344.8	3.22E-21	0.548	345.0	2.54E-21	0.542
345.2	1.60E-21	0.537	345.4	1.15E-21	0.531	345.6	8.90E-22	0.525	345.8	6.50E-22	0.520	346.0	5.09E-22	0.514
346.2	5.15E-22	0.508	346.4	3.45E-22	0.503	346.6	3.18E-22	0.497	346.8	3.56E-22	0.491	347.0	3.24E-22	0.485
347.2	3.34E-22	0.480	347.4	2.88E-22	0.474	347.6	2.84E-22	0.468	347.8	9.37E-22	0.463	348.0	9.70E-22	0.457
348.2	7.60E-22	0.451	348.4	6.24E-22	0.446	348.6	4.99E-22	0.440	348.8	4.08E-22	0.434	349.0	3.39E-22	0.428
349.2	1.64E-22	0.423	349.4	1.49E-22	0.417	349.6	8.30E-23	0.411	349.8	2.52E-23	0.406	350.0	2.57E-23	0.400
350.2	0.00E+00	0.394	350.4	5.16E-23	0.389	350.6	0.00E+00	0.383	350.8	2.16E-23	0.377	351.0	7.07E-23	0.371
351.2	3.45E-23	0.366	351.4	1.97E-22	0.360	351.6	4.80E-22	0.354	351.8	3.13E-21	0.349	352.0	6.41E-21	0.343
352.2	8.38E-21	0.337	352.4	1.55E-20	0.331	352.6	1.86E-20	0.326	352.8	1.94E-20	0.320	353.0	2.78E-20	0.314
353.2	1.96E-20	0.309	353.4	1.67E-20	0.303	353.6	1.75E-20	0.297	353.8	1.63E-20	0.291	354.0	1.36E-20	0.286
354.2	1.07E-20	0.280	354.4	9.82E-21	0.274	354.6	8.66E-21	0.269	354.8	6.44E-21	0.263	355.0	4.84E-21	0.257
355.2	3.49E-21	0.251	355.4	2.41E-21	0.246	355.6	1.74E-21	0.240	355.8	1.11E-21	0.234	356.0	7.37E-22	0.229
356.2	4.17E-22	0.223	356.4	1.95E-22	0.217	356.6	1.50E-22	0.211	356.8	8.14E-23	0.206	357.0	0.00E+00	0.200
Photolysis File = CCHOR														
260.0	2.00E-20	0.310	270.0	3.40E-20	0.390	280.0	4.50E-20	0.580	290.0	4.90E-20	0.530	295.0	4.50E-20	0.480
300.0	4.30E-20	0.430	305.0	3.40E-20	0.370	315.0	2.10E-20	0.170	320.0	1.80E-20	0.100	325.0	1.10E-20	0.040
330.0	6.90E-21	0.000												
Photolysis File = RCHO														
280.0	5.26E-20	0.960	290.0	5.77E-20	0.910	300.0	5.05E-20	0.860	310.0	3.68E-20	0.600	320.0	1.66E-20	0.360
330.0	6.49E-21	0.200	340.0	1.44E-21	0.080	345.0	0.00E+00	0.020						
Photolysis File = ACET-93C														
250.0	2.37E-20	0.760	260.0	3.66E-20	0.800	270.0	4.63E-20	0.640	280.0	5.05E-20	0.550	290.0	4.21E-20	0.300
300.0	2.78E-20	0.150	310.0	1.44E-20	0.050	320.0	4.80E-21	0.026	330.0	8.00E-22	0.017	340.0	1.00E-22	0.000
350.0	3.00E-23	0.000	360.0	0.00E+00	0.000									
Photolysis File = KETONE														
210.0	1.10E-21	1.000	220.0	1.20E-21	1.000	230.0	4.60E-21	1.000	240.0	1.30E-20	1.000	250.0	2.68E-20	1.000
260.0	4.21E-20	1.000	270.0	5.54E-20	1.000	280.0	5.92E-20	1.000	290.0	5.16E-20	1.000	300.0	3.44E-20	1.000
310.0	1.53E-20	1.000	320.0	4.60E-21	1.000	330.0	1.10E-21	1.000	340.0	0.00E+00	1.000			
Photolysis File = GLYOXAL1														
230.0	2.87E-21	1.000	235.0	2.87E-21	1.000	240.0	4.30E-21	1.000	245.0	5.73E-21	1.000	250.0	8.60E-21	1.000
255.0	1.15E-20	1.000	260.0	1.43E-20	1.000	265.0	1.86E-20	1.000	270.0	2.29E-20	1.000	275.0	2.58E-20	1.000
280.0	2.87E-20	1.000	285.0	3.30E-20	1.000	290.0	3.15E-20	1.000	295.0	3.30E-20	1.000	300.0	3.58E-20	1.000
305.0	2.72E-20	1.000	310.0	2.72E-20	1.000	312.5	2.87E-20	1.000	315.0	2.29E-20	1.000	320.0	1.43E-20	1.000
325.0	1.15E-20	1.000	327.5	1.43E-20	1.000	330.0	1.15E-20	1.000	335.0	2.87E-21	1.000	340.0	0.00E+00	1.000
Photolysis File = GLYOXAL2														
355.0	0.00E+00	1.000	360.0	2.29E-21	1.000	365.0	2.87E-21	1.000	370.0	8.03E-21	1.000	375.0	1.00E-20	1.000
380.0	1.72E-20	1.000	382.0	1.58E-20	1.000	384.0	1.49E-20	1.000	386.0	1.49E-20	1.000	388.0	2.87E-20	1.000
390.0	3.15E-20	1.000	391.0	3.24E-20	1.000	392.0	3.04E-20	1.000	393.0	2.23E-20	1.000	394.0	2.63E-20	1.000
395.0	3.04E-20	1.000	396.0	2.63E-20	1.000	397.0	2.43E-20	1.000	398.0	3.24E-20	1.000	399.0	3.04E-20	1.000
400.0	2.84E-20	1.000	401.0	3.24E-20	1.000	402.0	4.46E-20	1.000	403.0	5.27E-20	1.000	404.0	4.26E-20	1.000
405.0	3.04E-20	1.000	406.0	3.04E-20	1.000	407.0	2.84E-20	1.000	408.0	2.43E-20	1.000	409.0	2.84E-20	1.000
410.0	6.08E-20	1.000	411.0	5.07E-20	1.000	411.5	6.08E-20	1.000	412.0	4.86E-20	1.000	413.0	8.31E-20	1.000
413.5	6.48E-20	1.000	414.0	7.50E-20	1.000	414.5	8.11E-20	1.000	415.0	8.11E-20	1.000	415.5	6.89E-20	1.000
416.0	4.26E-20	1.000	417.0	4.86E-20	1.000	418.0	5.88E-20	1.000	419.0	6.69E-20	1.000	420.0	3.85E-20	1.000
421.0	5.67E-20	1.000	421.5	4.46E-20	1.000	422.0	5.27E-20	1.000	422.5	1.05E-19	1.000	423.0	8.51E-20	1.000
424.0	6.08E-20	1.000	425.0	7.29E-20	1.000	426.0	1.18E-19	1.000	426.5	1.30E-19	1.000	427.0	1.07E-19	1.000
428.0	1.66E-19	1.000	429.0	4.05E-20	1.000	430.0	5.07E-20	1.000	431.0	4.86E-20	1.000	432.0	4.05E-20	1.000
433.0	3.65E-20	1.000	434.0	4.05E-20	1.000	434.5	6.08E-20	1.000	435.0	5.07E-20	1.000	436.0	8.11E-20	1.000
436.5	1.13E-19	1.000	437.0	5.27E-20	1.000	438.0	1.01E-19	1.000	438.5	1.38E-19	1.000	439.0	7.70E-20	1.000
440.0	2.47E-19	1.000	441.0	8.11E-20	1.000	442.0	6.08E-20	1.000	443.0	7.50E-20	1.000	444.0	9.32E-20	1.000
445.0	1.13E-19	1.000	446.0	5.27E-20	1.000	447.0	2.43E-20	1.000	448.0	2.84E-20	1.000	449.0	3.85E-20	1.000
450.0	6.08E-20	1.000	451.0	1.09E-19	1.000	451.5	9.32E-20	1.000	452.0	1.22E-19	1.000	453.0	2.39E-19	1.000
454.0	1.70E-19	1.000	455.0	3.40E-19	1.000	455.5	4.05E-19	1.000	456.0	1.01E-19	1.000	457.0	1.62E-20	1.000
458.0	1.22E-20	1.000	458.5	1.42E-20	1.000	459.0	4.05E-21	1.000	460.0	4.05E-21	1.000	460.5	6.08E-21	1.000
461.0	2.03E-21	1.000	462.0	0.00E+00	1.000									
Photolysis File = MEGLYOX1														
220.0	2.10E-21	1.000	225.0	2.10E-21	1.000	230.0	4.21E-21	1.000	235.0	7.57E-21	1.000	240.0	9.25E-21	1.000
245.0	8.41E-21	1.000	250.0	9.25E-21	1.000	255.0	9.25E-21	1.000	260.0	9.67E-21	1.000	265.0	1.05E-20	1.000

Table A-3. (continued)

WL (nm)	Abs (cm^2)	QY	WL (nm)	Abs (cm^2)	QY	WL (nm)	Abs (cm^2)	QY	WL (nm)	Abs (cm^2)	QY	WL (nm)	Abs (cm^2)	QY
270.0	1.26E-20	1.000	275.0	1.43E-20	1.000	280.0	1.51E-20	1.000	285.0	1.43E-20	1.000	290.0	1.47E-20	1.000
295.0	1.18E-20	1.000	300.0	1.14E-20	1.000	305.0	9.25E-21	1.000	310.0	6.31E-21	1.000	315.0	5.47E-21	1.000
320.0	3.36E-21	1.000	325.0	1.68E-21	1.000	330.0	8.41E-22	1.000	335.0	0.00E+00	1.000			
Photolysis File = MEGLYOX2														
350.0	0.00E+00	1.000	354.0	4.21E-22	1.000	358.0	1.26E-21	1.000	360.0	2.10E-21	1.000	362.0	2.10E-21	1.000
364.0	2.94E-21	1.000	366.0	3.36E-21	1.000	368.0	4.21E-21	1.000	370.0	5.47E-21	1.000	372.0	5.89E-21	1.000
374.0	7.57E-21	1.000	376.0	7.99E-21	1.000	378.0	8.83E-21	1.000	380.0	1.01E-20	1.000	382.0	1.09E-20	1.000
384.0	1.35E-20	1.000	386.0	1.51E-20	1.000	388.0	1.72E-20	1.000	390.0	2.06E-20	1.000	392.0	2.10E-20	1.000
394.0	2.31E-20	1.000	396.0	2.48E-20	1.000	398.0	2.61E-20	1.000	400.0	2.78E-20	1.000	402.0	2.99E-20	1.000
404.0	3.20E-20	1.000	406.0	3.79E-20	1.000	408.0	3.95E-20	1.000	410.0	4.33E-20	1.000	412.0	4.71E-20	1.000
414.0	4.79E-20	1.000	416.0	4.88E-20	1.000	418.0	5.05E-20	1.000	420.0	5.21E-20	1.000	422.0	5.30E-20	1.000
424.0	5.17E-20	1.000	426.0	5.30E-20	1.000	428.0	5.21E-20	1.000	430.0	5.55E-20	1.000	432.0	5.13E-20	1.000
434.0	5.68E-20	1.000	436.0	6.22E-20	1.000	438.0	6.06E-20	1.000	440.0	5.47E-20	1.000	441.0	6.14E-20	1.000
442.0	5.47E-20	1.000	443.0	5.55E-20	1.000	443.5	6.81E-20	1.000	444.0	5.97E-20	1.000	445.0	5.13E-20	1.000
446.0	4.88E-20	1.000	447.0	5.72E-20	1.000	448.0	5.47E-20	1.000	449.0	6.56E-20	1.000	450.0	5.05E-20	1.000
451.0	3.03E-20	1.000	452.0	4.29E-20	1.000	453.0	2.78E-20	1.000	454.0	2.27E-20	1.000	456.0	1.77E-20	1.000
458.0	8.41E-21	1.000	460.0	4.21E-21	1.000	464.0	1.68E-21	1.000	468.0	0.00E+00	1.000			
Photolysis File = BZCHO														
299.0	1.78E-19	1.000	304.0	7.40E-20	1.000	306.0	6.91E-20	1.000	309.0	6.41E-20	1.000	313.0	6.91E-20	1.000
314.0	6.91E-20	1.000	318.0	6.41E-20	1.000	325.0	8.39E-20	1.000	332.0	7.65E-20	1.000	338.0	8.88E-20	1.000
342.0	8.88E-20	1.000	346.0	7.89E-20	1.000	349.0	7.89E-20	1.000	354.0	9.13E-20	1.000	355.0	8.14E-20	1.000
364.0	5.67E-20	1.000	368.0	6.66E-20	1.000	369.0	8.39E-20	1.000	370.0	8.39E-20	1.000	372.0	3.45E-20	1.000
374.0	3.21E-20	1.000	376.0	2.47E-20	1.000	377.0	2.47E-20	1.000	380.0	3.58E-20	1.000	382.0	9.90E-21	1.000
386.0	0.00E+00	1.000												
Photolysis File = ACROLEIN														
250.0	1.80E-21	1.000	252.0	2.05E-21	1.000	253.0	2.20E-21	1.000	254.0	2.32E-21	1.000	255.0	2.45E-21	1.000
256.0	2.56E-21	1.000	257.0	2.65E-21	1.000	258.0	2.74E-21	1.000	259.0	2.83E-21	1.000	260.0	2.98E-21	1.000
261.0	3.24E-21	1.000	262.0	3.47E-21	1.000	263.0	3.58E-21	1.000	264.0	3.93E-21	1.000	265.0	4.67E-21	1.000
266.0	5.10E-21	1.000	267.0	5.38E-21	1.000	268.0	5.73E-21	1.000	269.0	6.13E-21	1.000	270.0	6.64E-21	1.000
271.0	7.20E-21	1.000	272.0	7.77E-21	1.000	273.0	8.37E-21	1.000	274.0	8.94E-21	1.000	275.0	9.55E-21	1.000
276.0	1.04E-20	1.000	277.0	1.12E-20	1.000	278.0	1.19E-20	1.000	279.0	1.27E-20	1.000	280.0	1.27E-20	1.000
281.0	1.26E-20	1.000	282.0	1.26E-20	1.000	283.0	1.28E-20	1.000	284.0	1.33E-20	1.000	285.0	1.38E-20	1.000
286.0	1.44E-20	1.000	287.0	1.50E-20	1.000	288.0	1.57E-20	1.000	289.0	1.63E-20	1.000	290.0	1.71E-20	1.000
291.0	1.78E-20	1.000	292.0	1.86E-20	1.000	293.0	1.95E-20	1.000	294.0	2.05E-20	1.000	295.0	2.15E-20	1.000
296.0	2.26E-20	1.000	297.0	2.37E-20	1.000	298.0	2.48E-20	1.000	299.0	2.60E-20	1.000	300.0	2.73E-20	1.000
301.0	2.85E-20	1.000	302.0	2.99E-20	1.000	303.0	3.13E-20	1.000	304.0	3.27E-20	1.000	305.0	3.39E-20	1.000
306.0	3.51E-20	1.000	307.0	3.63E-20	1.000	308.0	3.77E-20	1.000	309.0	3.91E-20	1.000	310.0	4.07E-20	1.000
311.0	4.25E-20	1.000	312.0	4.39E-20	1.000	313.0	4.44E-20	1.000	314.0	4.50E-20	1.000	315.0	4.59E-20	1.000
316.0	4.75E-20	1.000	317.0	4.90E-20	1.000	318.0	5.05E-20	1.000	319.0	5.19E-20	1.000	320.0	5.31E-20	1.000
321.0	5.43E-20	1.000	322.0	5.52E-20	1.000	323.0	5.60E-20	1.000	324.0	5.67E-20	1.000	325.0	5.67E-20	1.000
326.0	5.62E-20	1.000	327.0	5.63E-20	1.000	328.0	5.71E-20	1.000	329.0	5.76E-20	1.000	330.0	5.80E-20	1.000
331.0	5.95E-20	1.000	332.0	6.23E-20	1.000	333.0	6.39E-20	1.000	334.0	6.38E-20	1.000	335.0	6.24E-20	1.000
336.0	6.01E-20	1.000	337.0	5.79E-20	1.000	338.0	5.63E-20	1.000	339.0	5.56E-20	1.000	340.0	5.52E-20	1.000
341.0	5.54E-20	1.000	342.0	5.53E-20	1.000	343.0	5.47E-20	1.000	344.0	5.41E-20	1.000	345.0	5.40E-20	1.000
346.0	5.48E-20	1.000	347.0	5.90E-20	1.000	348.0	6.08E-20	1.000	349.0	6.00E-20	1.000	350.0	5.53E-20	1.000
351.0	5.03E-20	1.000	352.0	4.50E-20	1.000	353.0	4.03E-20	1.000	354.0	3.75E-20	1.000	355.0	3.55E-20	1.000
356.0	3.45E-20	1.000	357.0	3.46E-20	1.000	358.0	3.49E-20	1.000	359.0	3.41E-20	1.000	360.0	3.23E-20	1.000
361.0	2.95E-20	1.000	362.0	2.81E-20	1.000	363.0	2.91E-20	1.000	364.0	3.25E-20	1.000	365.0	3.54E-20	1.000
366.0	3.30E-20	1.000	367.0	2.78E-20	1.000	368.0	2.15E-20	1.000	369.0	1.59E-20	1.000	370.0	1.19E-20	1.000
371.0	8.99E-21	1.000	372.0	7.22E-21	1.000	373.0	5.86E-21	1.000	374.0	4.69E-21	1.000	375.0	3.72E-21	1.000
376.0	3.57E-21	1.000	377.0	3.55E-21	1.000	378.0	2.83E-21	1.000	379.0	1.69E-21	1.000	380.0	8.29E-24	1.000
381.0	0.00E+00	1.000												

Table A-4. Values of chamber-dependent parameters used in the model simulations of the experiments for this study. [a]

Parm.	Value(s)	Discussion
k(1)	0.194 min^{-1}	Derived by fitting results of quartz tube NO_2 actinometry measurements to curve similar to that derived for other blacklight chambers by Carter et al (1995b). The results of the actinometry experiments carried out during this study were within the uncertainty range of this extrapolation.
k(O3W)	$1.5x10^{-4}$ min^{-1}	The results of the O_3 dark decay experiments in this chamber are consistent with the recommended default of Carter et al (1995b) for Teflon bag chambers in general.
k(N25I) k(N25S)	$2.8\ x10^{-3}$ min^{-1}, $1.5x10^{-6}$ - k_g ppm^{-1} min^{-1}	Based on the N_2O_5 decay rate measurements in a similar chamber reported by Tuazon et al. (1983). Although we previously estimated there rate constants were lower in the larger Teflon bag chambers (Carter and Lurmann, 1990, 1991), we now consider it more reasonable to use the same rate constants for all such chambers (Carter et al., 1995b).
k(NO2W) yHONO	$1.6x10^{-4}$ min^{-1} 0.2	Based on dark NO_2 decay and HONO formation measured in a similar chamber by Pitts et al. (1984). Assumed to be the same in all Teflon bag chambers (Carter et al, 1995b).
k(XSHC)	250 min^{-1}	Estimated by modeling pure air irradiations. Not an important parameter affecting model predictions except for pure air or NO_x-air runs.
RS/K1	$3.27x10^{6}$ $e^{-7297/T}$ ppm	Based on model simulations of n-butane - NO_x experiments. The temperature dependence is derived from simulating outdoor experiments as discussed by Carter et al. (1995b).
E-NO2/K1	0.03 ppb	Based on model simulations of pure air experiments.

[a] See Table A-2 for definitions of the parameters.